

# A complete sample of 21-cm absorbers at $z \sim 1.3$ : Giant Metrewave Radio Telescope Survey Using Mg II Systems

N. Gupta<sup>1</sup>\*, R. Srianand<sup>2</sup>, P. Petitjean<sup>3</sup>, P. Noterdaeme<sup>2</sup>, D. J. Saikia<sup>4</sup>

<sup>1</sup> Australia Telescope National Facility, CSIRO, Epping, NSW 1710, Australia

<sup>2</sup> IUCAA, Ganeshkhind, Pune 411007, India

<sup>3</sup> Université Paris 6, UMR 7095, Institut d'Astrophysique de Paris-CNRS, 98bis Boulevard Arago, 75014 Paris, France

<sup>4</sup> NCRA-TIFR, Ganeshkhind, Pune 411007, India

Accepted. Received; in original form

## ABSTRACT

We present the results of a systematic Giant Metrewave Radio Telescope (GMRT) survey of 21-cm absorption in a representative and unbiased sample of 35 strong Mg II systems in the redshift range:  $z_{\text{abs}} \sim 1.10 - 1.45$ , 33 of which have  $W_r \geq 1 \text{ \AA}$ . The survey using  $\sim 400$  hrs of telescope time has resulted in 9 new 21-cm detections and stringent 21-cm optical depth upper limits (median  $3\sigma$  optical depth per  $10 \text{ km s}^{-1}$  of 0.017) for the remaining 26 systems. This is by far the largest number of 21-cm detections from any single survey of intervening absorbers. Prior to our survey no intervening 21-cm system was known in the above redshift range and only one system was known in the redshift range  $0.7 \leq z \leq 1.5$ . We discuss the relation between the detectability of 21-cm absorption and various properties of UV absorption lines. We show that if Mg II systems are selected with the following criteria, Mg II doublet ratio  $\leq 1.3$  and  $W_r(\text{Mg I})/W_r(\text{Mg II}) \geq 0.3$ , then a detection rate of 21-cm absorption up to 90% can be achieved. We estimate  $n_{21}$ , the number per unit redshift of 21-cm absorbers with  $W_r(\text{Mg II}) > W_o$  and integrated optical depth  $T_{21} > T_o$  and show that  $n_{21}$  decreases with increasing redshift. In particular, for  $W_o = 1.0 \text{ \AA}$  and  $T_o > 0.3 \text{ km s}^{-1}$ ,  $n_{21}$  falls by a factor 4 from  $< z > = 0.5$  to  $< z > = 1.3$ . The evolution seems to be stronger for stronger Mg II systems. Using a subsample of systems for which high frequency VLBA images are available, we show that the effect is not related to the structure of the background radio sources and is most probably due to the evolution of the cold neutral medium filling factor in Mg II systems. We find no correlation between the velocity spread of the 21-cm absorption feature and  $W_r(\text{Mg II})$  at  $z \sim 1.3$ .

**Key words:** quasars: active – quasars: absorption lines –

## 1 INTRODUCTION

Observations of high- $z$  galaxies suggest that the global comoving star-formation rate density peaks at  $1 \leq z \leq 2$  and then sharply decreases towards  $z \sim 0$  (e.g. Madau et al. 1996, Hopkins 2004). The determination of the mass density of the gas and its content (molecules, dust and cold H I gas) over the same redshift range provides an independent and complementary understanding of the redshift evolution of star-formation at similar epochs. While the H I content of galaxies can be best probed by surveys of 21-cm emission, limited sensitivity of current radio telescopes does not allow them to reach beyond the local Universe (Zwaan et al. 2005 for  $z \sim 0$ ; Verheijen et al. 2007 and Catinella et al. 2008 for direct detections at  $z \sim 0.2$ ; Lah et al. 2007 for statistical

detection of H I at  $z \sim 0.24$ ). On the contrary, detection of H I in the spectra of distant QSOs in the form of damped Lyman- $\alpha$  absorption provides a luminosity unbiased way of probing the evolution of the H I content in the universe (Lanzetta et al. 1991; Wolfe et al. 1995; Storrie-Lombardi et al. 1996; Ellison et al. 2001; Peroux et al. 2003; Prochaska, Herbert-Ford & Wolfe, 2005; Rao, Turnshek & Nester, 2006; Prochaska & Wolfe 2008; Noterdaeme et al. 2009).

A major improvement in the DLA statistics at  $z \gtrsim 2$  has been achieved by the Sloan Digital Sky survey (SDSS). Spectroscopic catalogs are available for DR5 (see Prochaska & Wolfe 2008) and for DR7 (see Noterdaeme et al. 2009). For lower redshifts, initial detections of DLAs at  $z < 2$  were performed using the International Ultraviolet Explorer (IUE) and the Hubble Space Telescope (HST, Lanzetta, Wolfe & Turnshek, 1995; Jannuzi et al. 1998). However, a large number of low- $z$  DLAs have been identified after candidate DLAs

\* E-mail: Neeraj.Gupta@atnf.csiro.au

are pre-selected through the presence of strong metal absorption lines (Rao, Turnshek & Nestor, 2006; RTN06 from now on).

It is believed that physical conditions in the neutral gas associated with normal galaxies are influenced by the radiative and mechanical feedback from the in-situ star formation activity (McKee & Ostriker 1977). Thus, it is a good idea to investigate whether there is any relationship between the evolution of the star-formation rate density and the physical conditions in the H I gas probed by DLAs. Our understanding of physical conditions in DLAs at  $z \gtrsim 2$  is largely based on the analysis of H<sub>2</sub> and/or atomic fine-structure transitions. A systematic search for molecular hydrogen in DLAs at high redshifts ( $z_{\text{abs}} \gtrsim 1.8$ ), using Ultraviolet and Visual Echelle Spectrograph (UVES) at the Very Large Telescope (VLT) down to a detection limit of typically  $N(\text{H}_2) \sim 2 \times 10^{14} \text{ cm}^{-2}$ , has resulted in a detection in  $\sim 10\text{--}15\%$  of the cases (Ledoux, Petitjean & Srianand 2003; Noterdaeme et al 2008a). HD and CO molecules are detected in, respectively, two and one DLAs (Varshalovich et al. 2001; Noterdaeme et al. 2008b, Srianand et al. 2008a). The rotational excitation of the molecules and fine-structure excitations of C I and C II in these systems are consistent with the absorption lines originating from dense cold gas in radiative equilibrium with the star light produced by the in-situ star-formation (Srianand et al. 2000; Ge, Bechtold & Kulkarni 2001; Reimers et al. 2003; Srianand et al. 2005; Hirashita & Ferrara 2005; Cui et al. 2005; Noterdaeme et al. 2007a, 2007b). Absence of H<sub>2</sub> in most of the high- $z$  DLAs is consistent with the gas being either warm neutral or warm ionized (Petitjean, Srianand & Ledoux 2000; Srianand et al. 2005). The absorption lines of C II\* are detected in all the H<sub>2</sub> bearing DLAs (Srianand et al. 2005) and in roughly 50% of the DLAs without H<sub>2</sub> (Wolfe, Prochaska & Gawiser 2003; Wolfe, Gawiser & Prochaska 2003; Srianand et al. 2005; Wolfe et al. 2008). As C II\* is an important coolant, its column density combined with  $N(\text{H I})$  can be used to discuss the cooling rate in the absorbing gas and therefore the SFR associated with the DLA. Unfortunately for the time being the above mentioned tracers can not be used to probe the physical state of the absorbing gas at  $z \lesssim 1.8$  because the useful transitions are located below the atmospheric cut-off.

Most of our initial understanding of the physical state of H I gas in the Galactic interstellar medium (ISM) is based on the 21-cm absorption line (see Kulkarni & Heiles 1988 for details). It is widely believed that the spin temperature ( $T_s$ ) of the H I gas is a reliable tracer of the kinetic temperature (see Roy, Chengalur & Srianand 2006 for direct confirmation). The H I column density for an optically thin cloud that covers a fraction  $f_c$  of the background radio source is related to the 21-cm optical depth  $\tau(v)$  in a velocity interval  $v - v + dv$  and to the spin temperature ( $T_s$ ) by (e.g. Kulkarni & Heiles 1988)

$$N(\text{H I}) = 1.835 \times 10^{18} \frac{T_s}{f_c} \int \tau(v) dv \text{ cm}^{-2}. \quad (1)$$

In addition, the width of the 21-cm line detected in a high resolution spectrum yields a direct measurement of (or stringent upper limit on) the kinetic temperature. Thus detecting 21-cm absorption is important to probe the physical conditions in the interstellar medium of galaxies at intermediate redshifts.

RTN06 have shown that DLAs essentially have Mg II rest equivalent width,  $W_r(\text{Mg II} \lambda 2796) \geq 0.6 \text{ \AA}$ . Therefore, the search of 21-cm absorption in a sample of strong Mg II absorbers is an unique way to probe the redshift evolution of physical conditions in DLAs like absorption systems at low- $z$ . In the next Section we summarize the previous efforts to search for 21-cm absorption in DLAs and Mg II systems. Due to various practical reasons (e.g. frequency coverage of receivers, radio frequency interference, RFI) the redshift coverage is sparse and measurements are available only for a few systems, especially in the redshift range:  $1 \leq z \leq 2$ . The Giant Meterwave Radio Telescope (GMRT), with its very sensitive 610 MHz receiver, is the only radio telescope available at present in the *relatively* RFI-clean environment (e.g. compared to Green Bank Telescope or Westerbork Synthesis Radio Telescope) for covering part of this redshift range. In addition, the large number of publicly available high- $z$  QSO spectra from SDSS allow one to construct the large samples of Mg II absorbers suitable for the searches of DLAs/21-cm absorbers (cf. Section 3). Motivated by this we have conducted a systematic search for 21-cm absorption in a representative sample of Mg II systems in the redshift range  $1.10 \leq z \leq 1.45$  and discovered 9 new 21-cm absorbers. This is by far the highest number of detections from any single survey of intervening 21-cm absorption (see Srianand, Gupta & Petitjean 2007; Gupta et al. 2007 and Srianand et al. 2008b for preliminary results from the survey).

This paper is structured as follows. We give a brief summary of the past 21-cm searches performed by other groups in Section 2. In Section 3, we describe our sample and details of observations are presented in Section 4. In Section 5, we describe in detail the individual 21-cm absorbers detected in our survey. Detectability of 21-cm absorbers and its relationship to metal absorption equivalent widths, equivalent width ratios and structure of QSOs at radio wavelengths are discussed in Section 6. In Section 7, we derive the number density per unit redshift of 21-cm absorbers. Using the low- $z$  sample of Lane (2000) we investigate the redshift evolution of the number density of 21-cm absorbers. In Section 8, we explore the relationship between the velocity spread of 21-cm absorption and the equivalent width of the Mg II absorption line. Discussion of our results along with a summary are presented in Section 9.

## 2 BRIEF SUMMARY OF PREVIOUS 21-CM ABSORPTION LINE SURVEYS

There have been several systematic surveys for 21-cm absorption in DLAs and/or strong metal line absorption systems undertaken by various groups over the past two decades. Briggs & Wolfe (1983) searched 18 Mg II systems, with  $W_r(\text{Mg II}) \geq 0.5 \text{ \AA}$  and  $0.3 \leq z \leq 1.8$ , and detected two. Lane (2000), in her thesis work, searched 62 Mg II systems at  $0.2 \leq z \leq 0.9$  without imposing any equivalent widths cut-off and detected 21-cm absorption in 3 systems. Results of 21-cm searches are available for 7 DLAs at  $z \geq 2.8$  (Carilli et al. 1996; Kanekar & Chengalur 2003) with only one detection (Kanekar et al. 2007). Measurements are consistent with  $T_s \geq 1000 \text{ K}$ . There are five 21-cm detections reported in the literature for  $1.7 \leq z \leq 2.8$  [ $z_{\text{abs}} = 2.289$  towards TXS 0311+430 (York et al. 2007);

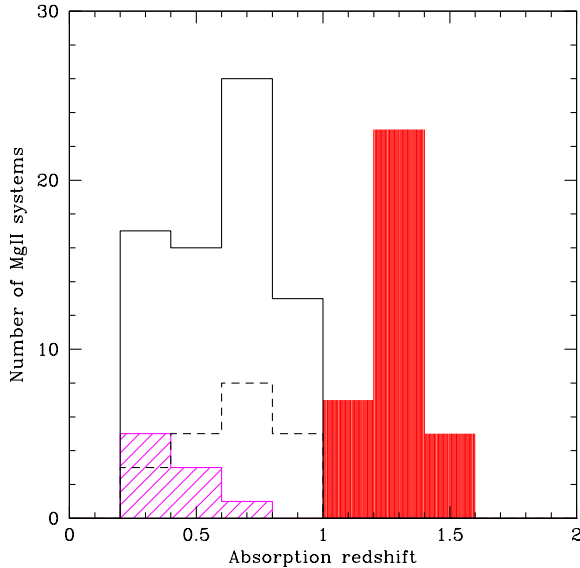


**Figure 1.** Redshift distribution of Mg II systems that were searched for 21-cm absorption. The filled histogram is the GMRT sample of 35 Mg II systems presented in this paper (33 of these absorption systems have  $W_r(\text{Mg II} \lambda 2796) \gtrsim 1 \text{ \AA}$ ). The solid line histogram is for the sample of Lane (2000). The hatched histogram corresponds to 21-cm detections in this sample. The distribution for the  $W_r(\text{Mg II} \lambda 2796) \geq 1 \text{ \AA}$  sub-set of these systems is given by the dashed line histogram.

$z_{\text{abs}} = 2.347$  towards B0438-436 (Kanekar et al. 2006);  $z_{\text{abs}} = 2.039$  towards B0458-020 (Wolfe et al. 1985);  $z_{\text{abs}} = 1.943$  towards 1157+014 (Wolfe & Briggs, 1981); and  $z_{\text{abs}} = 1.776$  towards 1331+170 (Wolfe & Davis, 1979)]. But non-detections are not systematically reported in this redshift range. At  $z < 0.9$ , Kanekar & Chengalur (2003) summarize 21-cm optical depths for 14 known DLAs and 12 detections (including their own observations of two DLAs namely PKS 1629+12 and PKS 2128-13). Curran et al. (2007) report the detection of a 21-cm absorption at  $z_{\text{abs}} = 0.656$  in the complex sight-line towards 3C336. In total 18 intervening 21-cm absorption systems are known till now.

We plot in Fig. 1 the redshift distribution of the Mg II absorption systems surveyed by Lane (2000). This is the only large survey at low- $z$  for which both detections and non-detections are systematically reported. It includes 62 observations using WSRT and 10 other systems from the literature satisfying their selection criterion (see Lane 2000 for details). The detections shown as a hatched histogram include detections reported in Lane (2000) together with detections from better quality data by Kanekar & Chengalur (2003) and Curran et al. (2007) for systems that were originally reported as non-detections. In the same figure, the filled histogram shows the distribution of Mg II systems in our GMRT sample. For equivalent width cutoff of  $\sim 1 \text{ \AA}$ , our GMRT sample has more than twice the number of systems investigated by Lane (2000). A detailed comparison of the results from low and high redshift samples will be discussed in Section 7.

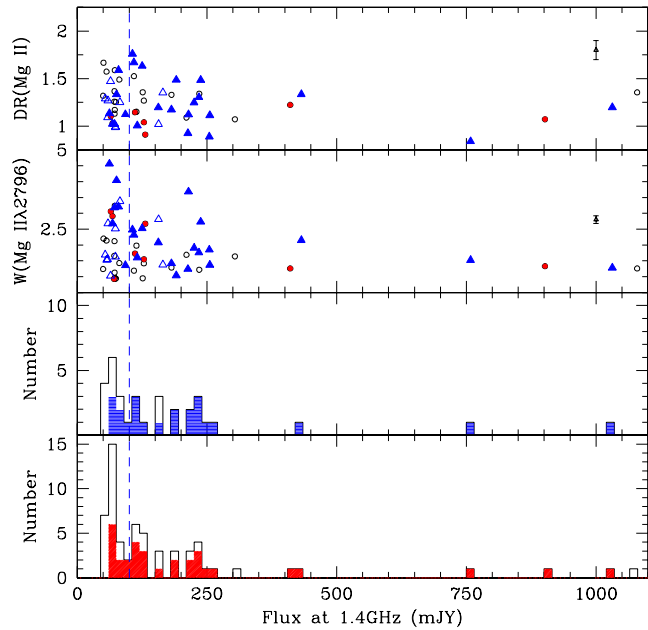


**Figure 2.** Top panels: The Mg II doublet ratios and Mg II $\lambda 2796$  equivalent widths in our sample are plotted against the 1.4 GHz peak flux density of the background source. Triangles are for systems from DR3 (P06) and circles are for additional systems in DR5. Filled and open symbols are for systems with and without GMRT observations. Typical error in the measurements are shown in these panels. Third and bottom panel: Distribution of radio flux densities in our sample. The shaded histograms gives the distributions of objects observed with GMRT.

### 3 SAMPLE OF Mg II SYSTEMS IN FRONT OF RADIO QUASARS

RTN06 have shown that DLAs can be preselected on the basis of the equivalent widths of Mg II, Fe II and Mg I absorption lines. Specifically, they found that  $36\% \pm 6\%$  of the Mg II absorbers with Fe II $\lambda 2600$  and Mg II $\lambda 2796$  rest equivalent widths greater than  $0.5 \text{ \AA}$  are DLAs. Motivated by this we have conducted a GMRT 21-cm absorption survey over the past two years in absorption systems selected on the basis of Mg II $\lambda 2796$  rest equivalent width in the redshift range  $1.10 \leq z \leq 1.45$ . The constraint on the redshift range comes from the frequency range covered by the GMRT 610 MHz receiver. Our sample is drawn from the identification of Mg II systems by Prochter, Prochaska & Burles (2006, hereafter P06) in SDSS DR3 and by us using our automatic procedure for additional systems in DR5. We do not make any further selection cut based on the equivalent widths of Fe II and Mg I absorption lines. Thus our candidate selection is based on  $W_r(\text{Mg II} \lambda 2796)$  alone.

There are 1953 Mg II systems in P06 with  $W_r(\text{Mg II} \lambda 2796) \geq 1.0 \text{ \AA}$  in the redshift range:  $1.10 \leq z \leq 1.45$ . By cross-correlating the corresponding QSO positions with the NRAO VLA Sky Survey (NVSS) radio catalog (Condon et al. 1998) we found 45 of these Mg II systems having background QSO with flux density at 1.4 GHz in excess of 50 mJy. We manually checked the SDSS spectra of all these sources to confirm the Mg II systems and remeasure

accurately the  $\lambda 2796$  rest equivalent width as well as other lines. This step is essential as the identifications of Mg II systems are not 100% complete and errors in the Mg II equivalent width measurement can be large (see discussion on this in P06) when one is using automatic procedures. We find that Mg II identification in one of the QSOs (i.e.  $z_{\text{abs}} = 1.109$  towards the very bright radio source J104833.69+600845.7) is spurious. While manually checking the SDSS spectra we detected an additional (i.e. not catalogued in P06) Mg II system at  $z_{\text{abs}} = 1.3739$  towards J123431.72+645556.5. Since this system has  $W_r(\text{Mg II} \lambda 2796) = 0.95 \pm 0.07$ , we included it in our sample as it satisfies the selection criteria of  $W_r \gtrsim 1 \text{\AA}$  within  $1\sigma$  and  $1.10 \leq z_{\text{abs}} \leq 1.45$ .

In order to minimize the possibility that the optical and radio sightlines are not identical we looked at the  $\sim 5''$  resolution radio images of the 44 remaining sources (with 45 absorption line systems) obtained in the Faint Images of the Radio Sky at Twenty-centimeters (FIRST) survey<sup>1</sup> (White et al. 1997). Eight sources in the list (J024534.05+010813.8, J095631.05+404628.2, J095908.31+024309.6, J103838.82+494736.8, J130907.98+522437.3, J141701.94+541340.6, J160846.76+374850.6 and J223334.89-075043.2) are resolved in the FIRST survey maps and the associated radio component closest to the optical source has a flux density less than 50 mJy. For this reason these sources are not included in our sample. In the case of J124538.35+551132.66 and J144553.46+034732.4 the radio peak of interest is more than  $8''$  away from the corresponding optical positions. As these separations are much larger than the astrometric accuracy of FIRST and SDSS we do not include these sources in our list. Another source, J100121.07+555355.8, is a gravitational lens commonly known as Q0957+561A,B. The two optical images are separated by  $\sim 6''$ . The radio structure is complex with core and jets. At 1420 MHz, the radio image is deconvolved into three components and none of the peaks coincide with any of the two optical images. The dominant radio component is located more than  $4''$  from the optical sources. For these reasons we did not include this source in our sample. Note that 21-cm absorption associated with the  $z_{\text{abs}} = 1.3911$  Mg II system has been searched for at GMRT by Kanekar & Chengalur (2003).

We ended up with a complete sample of 34 Mg II ( $W_r \gtrsim 1 \text{\AA}$ ) systems (in front of 33 radio sources) with flux density above 50 mJy from SDSS DR3. In our survey we have searched for 21-cm absorption in 24 of these systems. The distribution of the radio flux density in these sources is given in the third panel of Fig. 2. From this figure it is clear that we have searched for 21-cm absorption in all but the two systems with background sources having flux density greater than 100 mJy. We are only  $\sim 45\%$  complete for flux densities in the range 50–100 mJy.

Using an automatic procedure (similar to the one used by P06), we have identified 1548 additional strong Mg II systems in the same redshift range from DR5 of SDSS. Following the steps discussed above we have identified 29 systems

<sup>1</sup> FIRST images are not available for the two sources, namely, J021452.29+140527.4 and J123431.72+645556.5. We retain these in our sample.

in front of 29 QSOs having at least a  $S_{1.4\text{GHz}} > 50 \text{ mJy}$  component coinciding with the optical position in the FIRST image. Due to scheduling constraints, we could only cover 8 of these sources in our GMRT observations.

Therefore in total we have observed a sample of 32  $W_r \gtrsim 1 \text{\AA}$  Mg II systems in front of the 31 radio sources drawn from SDSS. In the bottom panel of Fig 2 we give the distribution of fluxes in our observed sample. In summary, we have observed, respectively,  $\sim 70\%$  (resp. 35%) of the available sources with flux densities  $S_{1.4\text{GHz}} > 100 \text{ mJy}$  (resp. in the range 50–100 mJy). From the top two panels of Fig 2 it is apparent that the distribution of  $W_r(\text{Mg II} \lambda 2796)$  and Mg II doublet ratio (DR) in the systems observed with GMRT (filled circles) represent the parent distribution well. The two distribution Kolmogorov-Smirnov test (KS test) gives the probability of 70% and 36% respectively for the distribution of  $W_r(\text{Mg II} \lambda 2796)$  and DR(Mg II) in the sources with GMRT observations to represent the distribution of the parent population. *Therefore, despite incompleteness in our survey towards low flux density levels (i.e.  $< 100 \text{ mJy}$ ), the sample is representative of the parent population as far as  $W_r(\text{Mg II} \lambda 2796)$  and DR(Mg II) are concerned.*

In addition, we have observed three more sources i.e. J010826.84–003724.1 (York et al. 2006), and J0240-2309 and J160456.14–001907.1 (Lanzetta et al. 1987) because they have a total flux density at 610 MHz in excess of 1 Jy and are associated with strong Mg II absorptions. We notice that addition of these systems (that were observed in the early stages of our survey) does not change the statistical conclusions drawn above. Thus, in total we have observed 35 Mg II systems, 33 of which have  $W_r(\text{Mg II}) \gtrsim 1 \text{\AA}$ , to search for 21-cm absorption. In Table 1 we give the list of observed sources together with the emission redshift,  $z_{\text{em}}$  in column 2, the absorption redshift ( $z_{\text{abs}}$ ) in column 3, the rest equivalent widths of Mg II  $\lambda\lambda 2796, 2803$  (columns 4 and 5), Mg I  $\lambda 2852$  (column 6) and Fe II  $\lambda 2600$  (column 7), the radio flux density at 1420 MHz (column 8), morphology of the radio sources (column 9) and the origin of the Mg II systems (column 10). The equivalent width estimates in Table 1 were obtained by integrating the absorption over the absorption profile. For consistency these measurements were compared against estimates from Voigt profile fits. Differences of the order of  $0.2 \text{\AA}$  or less were found between estimates from these methods. This is similar to uncertainties ( $\sim 0.3 \text{\AA}$ ) from estimating equivalent widths by automatic procedures (see P06).

Preliminary results from the first phase of the GMRT survey reporting 3 new detections in 10 systems were presented in Gupta et al. 2007 (see also Srianand, Gupta & Petitjean, 2007 for details regarding J0240–2309). Detailed analysis of two detections from our survey with strong signatures of dust reddening is presented in Srianand et al. (2008b). Here we present the results for the entire survey.

## 4 GMRT OBSERVATIONS

We observed 35 Mg II systems with GMRT 610-MHz band using in total  $\sim 400$  hrs of telescope time. Details of the observations are given in Table 2. For our survey, we have usually used the 1 MHz baseband bandwidth split into 128 frequency channels yielding a spectral resolution of  $\sim 4 \text{ km s}^{-1}$ .

**Table 1.** Sample of Mg II systems observed with GMRT.

Source name	$z_{\text{em}}$	$z_{\text{abs}}$	$W_r(\text{Mg II}\lambda 2796)$ (Å)	$W_r(\text{Mg II}\lambda 2803)$ (Å)	$W_r(\text{Mg I}\lambda 2852)$ (Å)	$W_r(\text{Fe II}\lambda 2600)$ (Å)	Flux (mJy)	Morp.	Ref.
(1)	(2)	(3)	(4)	(5)	(6)	(7)	(8)	(9)	(10)
J010826.84-003724.1	1.373	1.3710	0.43±0.05	0.39±0.05	0.20±0.05	0.33±0.06	894.9	C	Y
J015454.36-000723.2	1.828	1.1803	1.37±0.19	1.23±0.19	<0.22	0.65±0.26	245.8	C	P
J021452.29+140527.4	2.178	1.4463	2.53±0.22	1.55±0.19	1.04±0.23	1.28±0.23	119.5	CN	P
J0240-2309 <sup>†</sup>	2.223	1.3647	1.85±0.002	1.65±0.002	0.27±0.002	0.87±0.003	6027	C <sup>‡</sup>	L
J025928.51-001959.9	2.000	1.3370	1.76±0.04	1.35±0.05	<0.05	0.36±0.05	226.7	C	P
J074237.38+394435.6	2.200	1.1485	2.48±0.41	1.41±0.35	<0.26	<0.69	99.3	C	P
J074809.46+300630.5	1.695	1.4470	3.68±0.06	3.28±0.07	0.85±0.08	2.17±0.08	200.4	C	P
J080248.43+291734.1	2.380	1.3648	1.04±0.19	0.70±0.16	<0.79	<0.23	190.4	C	P
J080442.23+301237.0	1.452	1.1908	1.28±0.05	1.07±0.06	0.19±0.06	1.05±0.07	1040	R	P
J080839.66+495036.5	1.436	1.4071	1.33±0.09	1.24±0.08	0.48±0.12	0.60±0.12	846.8	C	T
J081247.78+252242.0	1.803	1.3683	3.18±0.10	3.11±0.11	0.87±0.12	2.22±0.14	69.6	C?	P
J084506.24+425718.3	2.095	1.1147	1.24±0.09	1.34±0.09	<0.11	0.87±0.09	203.4	C	P
J085042.24+515911.7	1.894	1.3265	4.56±0.12	4.02±0.12	2.19±0.12	3.44±0.15	61.2	C	P
J085244.74+343540.4	1.655	1.3095	2.91±0.11	2.83±0.11	1.27±0.12	2.26±0.18	66.7	C	T
J095327.95+322551.6	1.575	1.2372	1.55±0.05	1.49±0.05	0.35±0.06	1.18±0.08	127.4	C	T
J100842.71+621955.7	1.875	1.2080	4.04±0.22	3.03±0.20	1.37±0.30	2.38±0.28	73.8	R	P
J101742.63+535635.0*	1.397	1.3055	2.68±0.10	2.62±0.11	0.70±0.11	1.98±0.14	64.0	R	P
J102258.41+123429.7	1.727	1.2505	3.06±0.07	2.77±0.08	0.87±0.07	2.45±0.11	64.6	T	T
J105813.05+493936.1	2.396	1.2120	1.91±0.23	1.53±0.25	0.84±0.20	0.88±0.34	215.6	C	P
J112657.65+451606.3	1.811	1.3022	1.26±0.05	1.03±0.05	0.20±0.05	0.38±0.05	374.7	C	T
J114521.32+045526.7	1.342	1.3433	2.15±0.11	1.61±0.12	1.29±0.14	1.40±0.17	413.1	R	P
J120854.25+544158.1	1.344	1.2110	1.85±0.25	2.08±0.26	<0.36	1.22±0.35	236.1	C	P
J123256.60+572214.1	2.118	1.3429	2.32±0.19	1.39±0.20	<0.19	1.53±0.18	107.6	C	P
J123431.73+645556.5	3.036	1.3739	0.95±0.07	0.84±0.07	<0.08	0.63±0.07	88.9	CN	M
		1.3829	1.36±0.07	1.21±0.07	<0.09	0.74±0.07	"	"	P
J132901.41+105304.9	1.933	1.1645	1.73±0.18	1.51±0.17	<0.19	1.11±0.17	106.9	C?	T
J141104.25-030043.3	1.531	1.4160	2.08±0.11	1.74±0.12	0.69±0.13	1.66±0.13	163.0	R	P
J145633.42+000555.5	1.835	1.3512	3.21±0.21	2.02±0.19	<0.20	1.46±0.26	77.8	R	P
J150823.71+334700.7	2.208	1.1650	2.67±0.08	2.93±0.07	0.79±0.09	1.59±0.12	130.3	C	T
J151005.88+595853.3	1.720	1.3720	1.42±0.07	1.21±0.07	<0.07	0.69±0.10	181.0	D	P
J160456.14-001907.1	1.629	1.3245	0.67±0.05	0.68±0.05	<0.05	0.51±0.05	301.6	T	L
J162346.23+071854.9	1.648	1.3350	0.93±0.06	0.91±0.06	0.13±0.05	0.68±0.06	69.3	C	T
J231222.36-010924.8	1.431	1.4262	2.73±0.24	1.84±0.24	0.46±0.45	1.25±0.60	237.7	R	P
J234023.66-005326.9	2.085	1.3603	1.60±0.04	1.59±0.04	0.50±0.04	1.18±0.04	114.2	C	P
J235810.87-102008.7	1.638	1.1726	1.52±0.15	1.81±0.14	0.50±0.14	1.11±0.16	730.7	C	P

Col. 1: SDSS source name; col. 2: QSO emission redshift; col. 3: Absorption redshift of Mg II systems as determined from Mg II $\lambda\lambda 2796, 2803$ , Mg I $\lambda 2852$  and Fe II $\lambda 2600$  absorption lines; cols. 4, 5, 6, 7: Rest equivalent widths or  $1\sigma$  limit of Mg II $\lambda 2796$ , Mg II $\lambda 2803$ , Mg I $\lambda 2852$ , Fe II $\lambda 2600$  absorption lines respectively; col. 8: Peak flux density at 1.4 GHz as measured from FIRST (or NVSS when FIRST image is not available) survey, col. 9: Radio morphology as determined from FIRST (or NVSS) where C=compact at the FIRST resolution ( $\sim 5''$ ), CN=compact at NVSS resolution ( $\sim 45''$ ), R=resolved in the FIRST image, D=double lobed and T=triple radio source, and col. 10: Origin of the Mg II systems, where Y is for York et al. (2006), P is for P06, L for Lanzetta et al. (1987), T for ‘this paper’ i.e. drawn from SDSS using a procedure developed by one of us and M is for detected while manually checking the SDSS spectra for other systems.

<sup>†</sup> Absorption line equivalent widths for this system are estimated from the VLT UVES data presented in Srianand et al. (2007).

<sup>‡</sup> Source is not covered by the FIRST and NVSS surveys but is a VLA phase calibrator for A, B, C and D configurations.

\* This source is extended in FIRST but compact in our GMRT image.

Broader (2 MHz for J0804+3012) and narrower (0.5 MHz for J2358-1020 and 0.25 MHz for J2340-0053) bandwidths were used as well for confirming the detected 21-cm absorptions. During each observations, the local oscillator chain was tuned to centre the baseband at the redshifted 21-cm frequency defined by the mean redshift estimated from the Mg II and other absorption lines detected in the SDSS spectrum. Data were acquired in the two circular polarization channels called RR and LL. We typically observed each absorption line system for 8 hrs which included calibration

overheads. For flux and bandpass calibration we observed one of the standard flux density calibrators 3C 48, 3C 147 and 3C 286 for 10-15 mins every two hours. A phase calibrator was also observed for 10 mins every  $\sim 40$  mins to get reliable phase solutions. Total on-source time after excluding the telescope set-up time and calibration overheads are provided in Table 2.

GMRT data were reduced using the NRAO Astronomical Image Processing System (AIPS) following the standard procedures as described in Gupta et al. (2006). After the

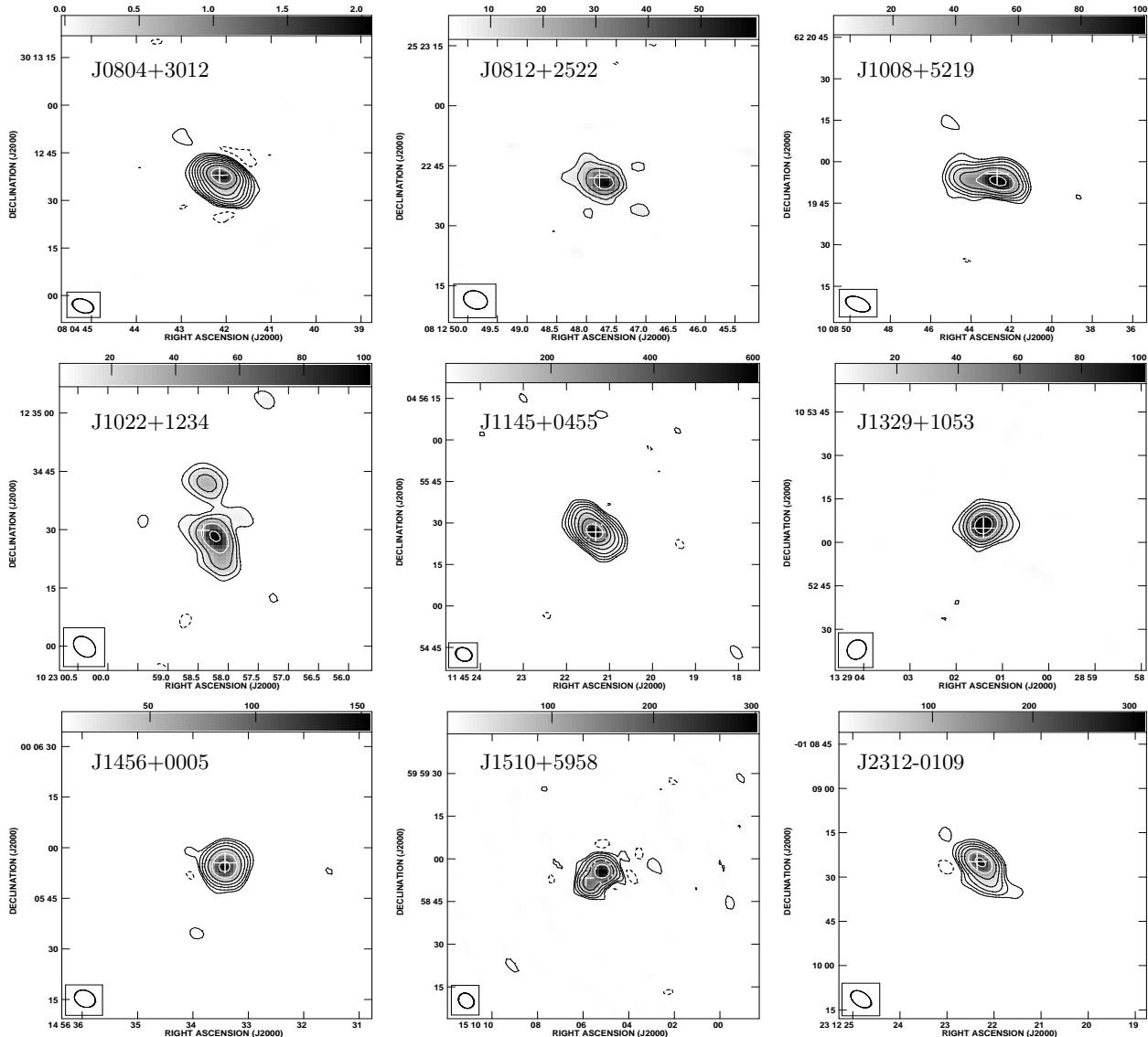


**Figure 3.** GMRT maps of sources resolved in our observations with contour levels as  $n \times (-1, 1, 2, 4, \dots)$  mJy beam $^{-1}$ . J0804+3012: 0.84 mJy beam $^{-1}$  rms and beam of  $6.36'' \times 4.09''$ , position angle PA=67° and n=4.0. J0812+2522: 0.90 mJy beam $^{-1}$  rms and beam of  $5.60'' \times 4.37''$ , PA=66° and n=5.0. J1008+5219: 0.51 mJy beam $^{-1}$  rms and beam of  $8.87'' \times 4.92''$ , P.A.=67° and n=1.6. J1022+1234: 0.90 mJy beam $^{-1}$  rms and beam of  $6.13'' \times 4.49''$ , PA=45° and n=6.0. J1145+0455: 0.90 mJy beam $^{-1}$  rms and beam of  $5.85'' \times 4.70''$ , PA=63° and n=3.0. J1329+1053: 0.70 mJy beam $^{-1}$  rms and beam of  $6.85'' \times 5.88''$ , PA=−26° and n=3.2. J1456+0005: 0.48 mJy beam $^{-1}$  rms and beam of  $5.93'' \times 4.78''$ , PA=59° and n=2.0. J1510+5958: 1.10 mJy beam $^{-1}$  rms and beam of  $5.67'' \times 4.71''$ , PA=36° and n=6.0. J2312-0109: 0.95 mJy beam $^{-1}$  rms and beam of  $7.38'' \times 4.66''$ , PA=53° and n=4.0.

initial flagging and calibration, source and calibrator data were examined to flag and exclude the baselines and timestamps affected by Radio Frequency Interference (RFI). Applying complex gains and bandpass obtained using the flux and phase calibrators, a continuum map of the source was made using absorption-free channels. Using this map as a model, self-calibration complex gains were determined and applied to all the frequency channels. The same continuum map was then used to subtract the continuum emission from the dataset. This continuum subtracted dataset was then imaged separately in stokes RR and LL to get 3-dimensional (with third axis as frequency) data cubes. The spectra at the quasar positions were extracted from these cubes and com-

pared for consistency. If necessary a first-order cubic-spline was fitted to remove the residual continuum from spectra. The two polarization channels were then combined to get the final stokes I spectrum, which was then shifted to heliocentric frame.

We have obtained useful radio spectra for 35 Mg II systems in front of 34 radio sources. Of these 34 radio sources 20 are compact in FIRST (deconvolved sizes  $< 2''$ ) and our 610 MHz images. These are assigned morphology C in Tables 1 and 3. Of the remaining 14 sources, for two sources (i.e. J0214+1405 and J1234+6455) FIRST images are not available. Both sources are compact in NVSS and our GMRT 610-MHz images. Radio emission associated with

**Table 3.** Observational results for Mg II systems observed with GMRT.

Source name	$z_{\text{abs}}$	Morph.	Peak Flux (mJy)	$\delta v$ ( $\text{km s}^{-1}$ )	Spectral rms ( $\text{mJy b}^{-1} \text{ch}^{-1}$ )	$\tau$	$\tau_{3\sigma,10}$	$\int \tau dv$ ( $\text{km s}^{-1}$ )
(1)	(2)	(3)	(4)	(5)	(6)	(7)	(8)	(9)
J0108-0037	1.3710	C	1276	3.9	2.9	0.070	0.003	1.29
J0154-0007	1.1803	C	154	3.6	1.7	<0.011	0.016	<0.17
J0214+1405	1.4463	C	220	4.0	2.7	<0.012	0.025	<0.26
J0240-2309	1.3647	C	5100	3.9	5.2	<0.001	0.002	<0.02
J0259-0019	1.3370	C	149	3.9	2.4	<0.016	0.027	<0.28
J0742+3944	1.1485	C	152	3.5	1.9	<0.013	0.034	<0.36
J0748+3006	1.4470	C	347	4.0	3.5	<0.010	0.017	<0.18
J0802+2917	1.3648	C	404	3.9	1.3	<0.003	0.006	<0.06
J0804+3012	1.1908	R	2069	7.2	1.5	0.006	0.002	0.39
J0808+4950	1.4071	C	754	4.0	1.2	0.008	0.002	0.10
J0812+2522	1.3683	R	59.1	3.9	1.2	<0.020	0.036	<0.38
J0845+4257	1.1147	C	224	3.5	3.0	<0.013	0.026	<0.27
J0850+5159	1.3265	C	64.0	3.8	1.2	0.503	0.038	15.3
J0852+3435	1.3095	C	51.2	3.8	0.8	0.143	0.036	6.91
J0953+3225	1.2372	C	148	3.7	1.8	<0.015	0.020	<0.22
J1008+6219	1.2080	R	132	3.6	1.0	<0.008	0.014	<0.15
J1017+5356	1.3055	R	127	3.8	2.3	<0.018	0.036	<0.38
J1022+1234	1.2505	T	109	3.7	1.2	<0.011	0.020	<0.21
J1058+4939	1.2120	C	437	3.6	1.3	0.020	0.005	0.41
J1126+4516	1.3022	C	356	3.8	1.4	<0.004	0.008	<0.08
J1145+0455	1.3433	R	717	3.9	2.4	<0.003	0.006	<0.07
J1208+5441	1.2110	C	274	3.7	1.5	<0.005	0.009	<0.10
J1232+5722	1.3429	C	221	3.9	1.4	<0.007	0.011	<0.12
J1234+6455	1.3739	C	141	3.9	1.3	<0.009	0.017	<0.18
		C	139	3.9	1.4	<0.010	0.017	<0.18
J1329+1053	1.1645	R	171	3.6	2.6	<0.015	0.034	<0.36
J1411-0300	1.4160	R	244	4.0	3.0	<0.012	0.026	<0.28
J1456+0005	1.3512	R	152	3.9	1.0	<0.007	0.014	<0.15
J1508+3347	1.1650	C	219	3.6	2.4	<0.007	0.022	<0.23
J1510+5958	1.3720	D	173	3.9	1.4	<0.008	0.016	<0.17
J1604-0019	1.3245	T	375	3.8	3.9	<0.010	0.019	<0.20
J1623+0718	1.3350	C	142	3.9	1.0	0.040	0.013	0.91
J2312-0109	1.4262	R	310	4.0	2.4	<0.008	0.015	<0.16
J2340-0053	1.3603	C	43.4	1.0	2.3	0.754	0.042	2.50
J2358-1020	1.1726	C	432	1.8	2.5	0.035	0.007	0.23

Col. 1: Source name; col. 2: Mg II absorption redshift; col. 3: Morphology of the radio source as determined from our observations; col. 4: Peak flux density in mJy; col. 5 and 6: Spectral resolution in  $\text{km s}^{-1}$  and spectral rms in  $\text{mJy beam}^{-1} \text{channel}^{-1}$ ; col. 7: Maximum of optical depth in one channel or  $1\sigma$  limit to it; col. 8:  $3\sigma$  optical depth limit for spectra smoothed to  $\sim 10 \text{ km s}^{-1}$ ; col. 9: integrated 21-cm optical depth or  $3\sigma$  upper limit in case of non-detections considering  $\delta v=10 \text{ km s}^{-1}$ .

J0214+1405 in our GMRT image (with beam  $5.5'' \times 4.6''$  and PA= $57^\circ$ ) is well represented by a Gaussian component implying a deconvolved size of  $2.5'' \times 1.6''$  with position angle  $56^\circ$ . Despite the deconvolved radio source size being slightly greater than  $2''$ ,  $>90\%$  of the total emission is contained in the above mentioned Gaussian component, so we consider this source to be compact. Gaussian deconvolution of J1234+6455 yields a size of  $0.7'' \times 0.0''$  with position angle  $12^\circ$  implying that the source is compact. This source is also compact in sub-arcsecond scale CLASS images at 8.4 GHz. Thus there are 22 sources compact at arcsec scales in our sample and 23 Mg II systems along their lines of sight with GMRT data. From Table 3 one can see eight (i.e.  $\sim 35\%$ ) of these systems show detectable 21-cm absorption.

Eleven sources in our sample show extensions in our GMRT continuum maps (see Fig. 3 in this article and Fig. 4 in Gupta et al. 2007). For 8 of these sources spectra were

extracted at the position of the peak flux that also coincides well with the optical position. For the three remaining sources (J1604-0019, J1411-0300 and J1510+5958) we also extracted spectra from the hot spots that are resolved from the core in our GMRT observations. In none of these cases we have detected 21-cm absorption towards hot spots. We address the issue of radio morphology of our target sources and its influence on the detectability of 21-cm absorption in following sections.

Absorption profiles of the nine newly discovered 21-cm absorbers are presented in Fig. 4 whereas spectra with no detectable 21-cm absorption are shown in Fig. 5. Results are summarised in Table 3. In the 3rd to 6th columns of this table we provide the morphology, the peak flux ( $F_P$ ) measured in our GMRT 610 MHz continuum image, the velocity resolution ( $\delta v$ ) and the measured spectral rms. In the seventh column, we provide the maximum optical depth per channel

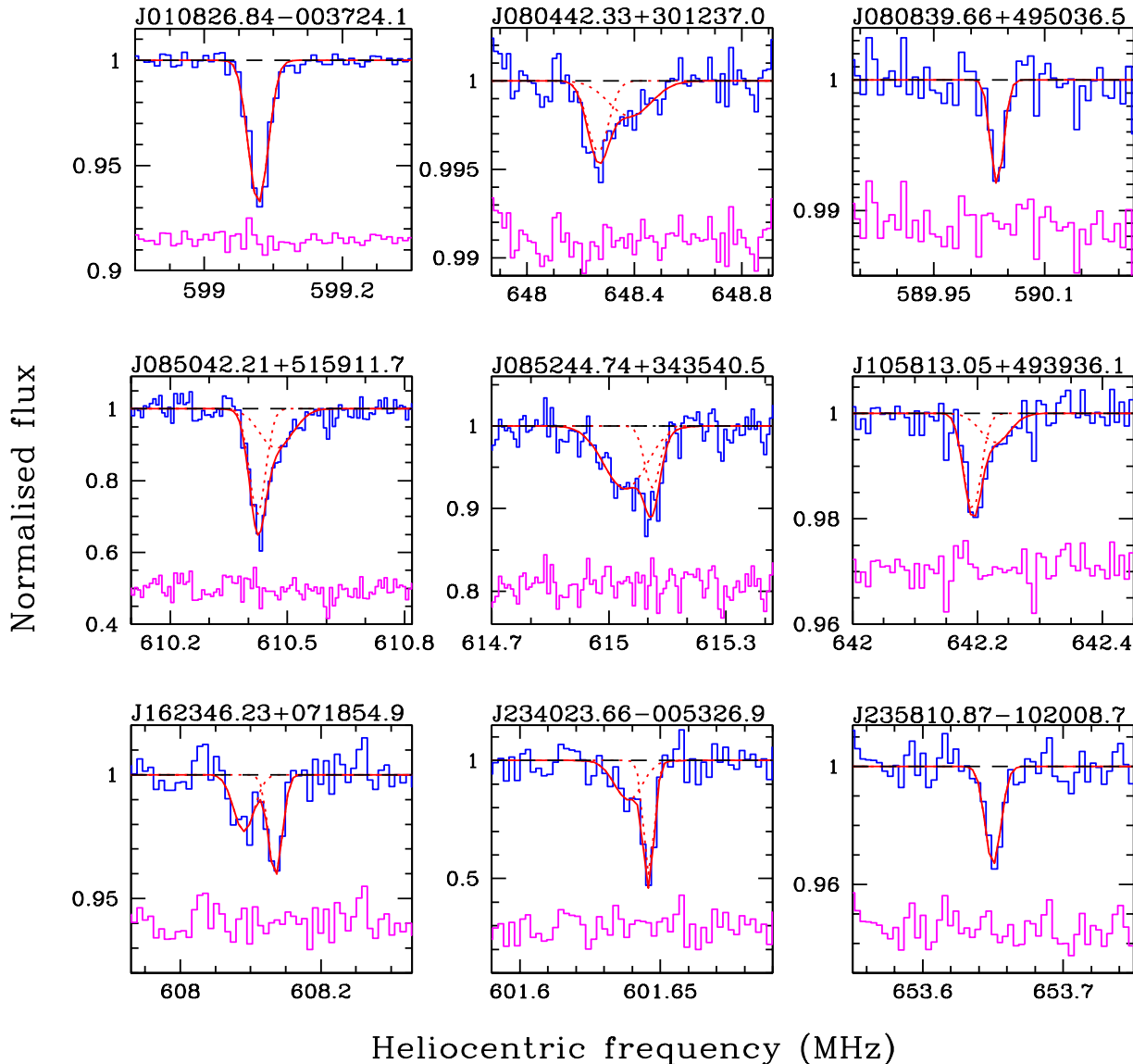


**Figure 4.** GMRT spectra of detected 21-cm absorption lines. Individual Gaussian components and resultant fits to the absorption profiles are overplotted as dotted and continuous lines respectively. Residuals, on an offset arbitrarily shifted for clarity, are also shown.

or the  $1\sigma$  limit on it. The next column gives the  $3\sigma$  optical depth limit obtained as follows:  $\tau_{3\sigma} = -\ln(1 - 3\Delta F/F_P)$ , where  $F_P$  is the peak flux and  $\Delta F$  is the spectral rms for the spectrum smoothed to  $10 \text{ km s}^{-1}$  resolution. This smoothing velocity scale is chosen to enable comparative studies with the existing low redshift (i.e.  $z_{\text{abs}} \leq 1.0$ ) measurements (see Section 7). In the case of detections, we measure this quantity in the line free spectral range. The last column in the table gives the integrated optical depth or the limit on it. In the later case we used a Gaussian width of  $10 \text{ km s}^{-1}$  for the integration (i.e.  $10.6 \times \tau_{3\sigma}$ ).

For detections, it is important to rule out the possibility of false identification even in case of good redshift coincidence. For spectra with high SNR (i.e. 21-cm absorption lines towards J0108-0037, J0850+5159 and J1058+4939) we split the data into different time and UV ranges and

check for consistency of the spectra. We also compared the spectra with spectra of other bright sources in the field. For spectra of poor SNR or when the narrow absorption line feature is spread over only one or two frequency channels (i.e. along the lines of sight towards J0804+3012, J0808+4950, J0852+3435, J1623+0718, J2340-0053 and J2358-1020), observations were repeated at a different epoch. In all cases we observed a consistent absorption profile at a frequency that is in good agreement with the Doppler shift expected from the heliocentric motion. For J0808+4950, J0852+3435 and J1623+0718 spectra at different epochs were obtained at the same spectral resolution ( $\sim 4 \text{ km s}^{-1}$ ) and the final spectra presented in Fig. 4 are weighted averages of these. The absorption line system towards J0804+3012 was observed three times. The later two observations were done using 2 MHz bandwidth split into 128 channels to obtain a wider

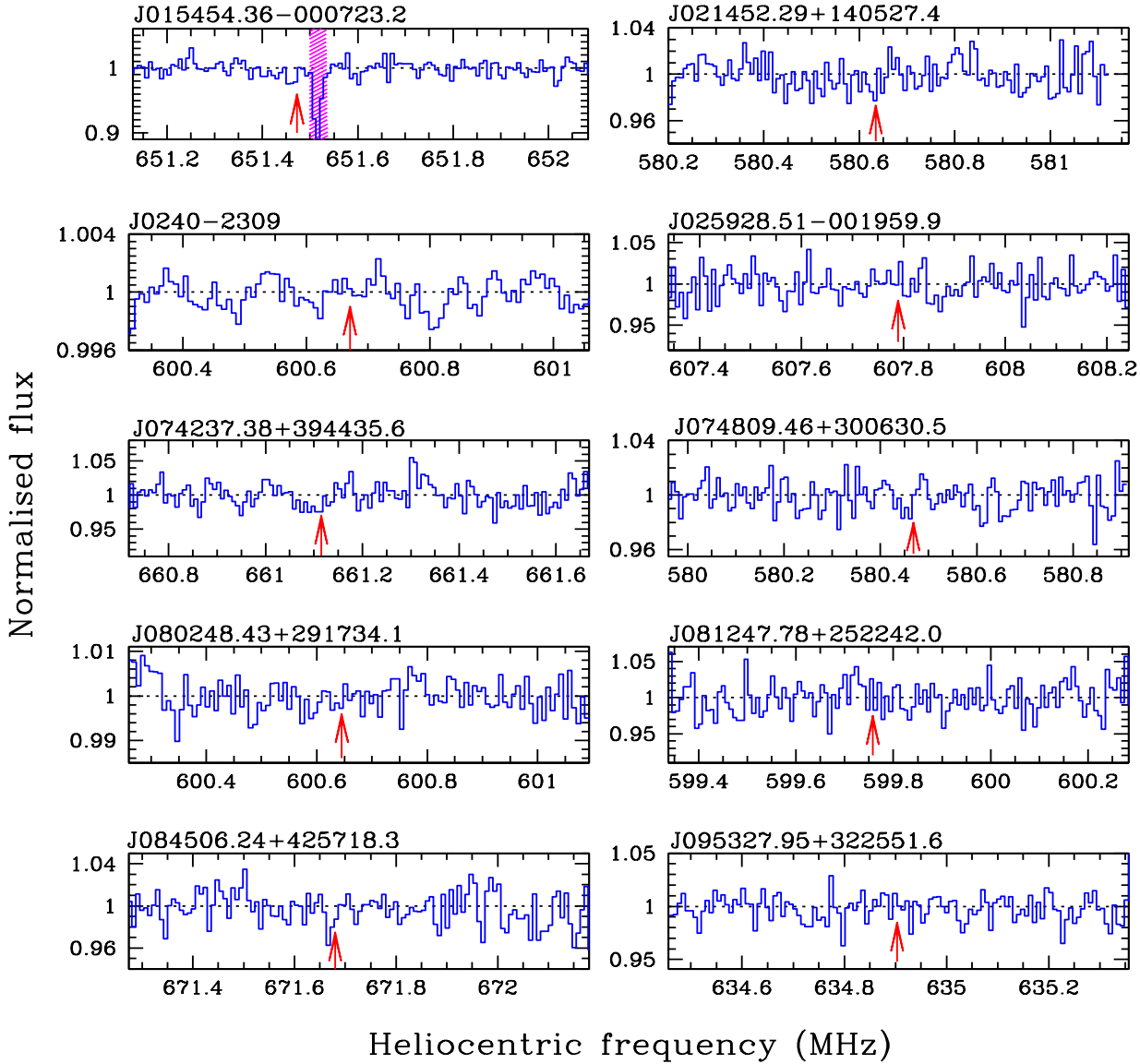


**Figure 5.** GMRT spectra of sources with non-detection. Arrows mark the expected positions of 21-cm absorption lines based on metal absorption lines. The shaded regions mark frequency ranges affected by RFI. The  $z_{\text{abs}}=1.3739$  and  $1.3829$  absorbers towards J1234+6455 are referred to as A and B respectively. For J1411-0300, P1 and P2 correspond to spectrum towards two peaks (see Gupta et al. 2007 for detail). The spectra toward northern and southern radio peaks of J1510+5958 are marked as N and S.

spectral coverage. The final spectrum presented here was obtained by smoothing the spectrum from the first observing run and combining this with the later two spectra of spectral resolution  $\sim 7 \text{ km s}^{-1}$  (see also Gupta et al. 2007). Narrow 21-cm absorption profiles detected towards J2340-0053 and J2358-1020 were reobserved at higher spectral resolution. Here, we present only the highest resolution spectra.

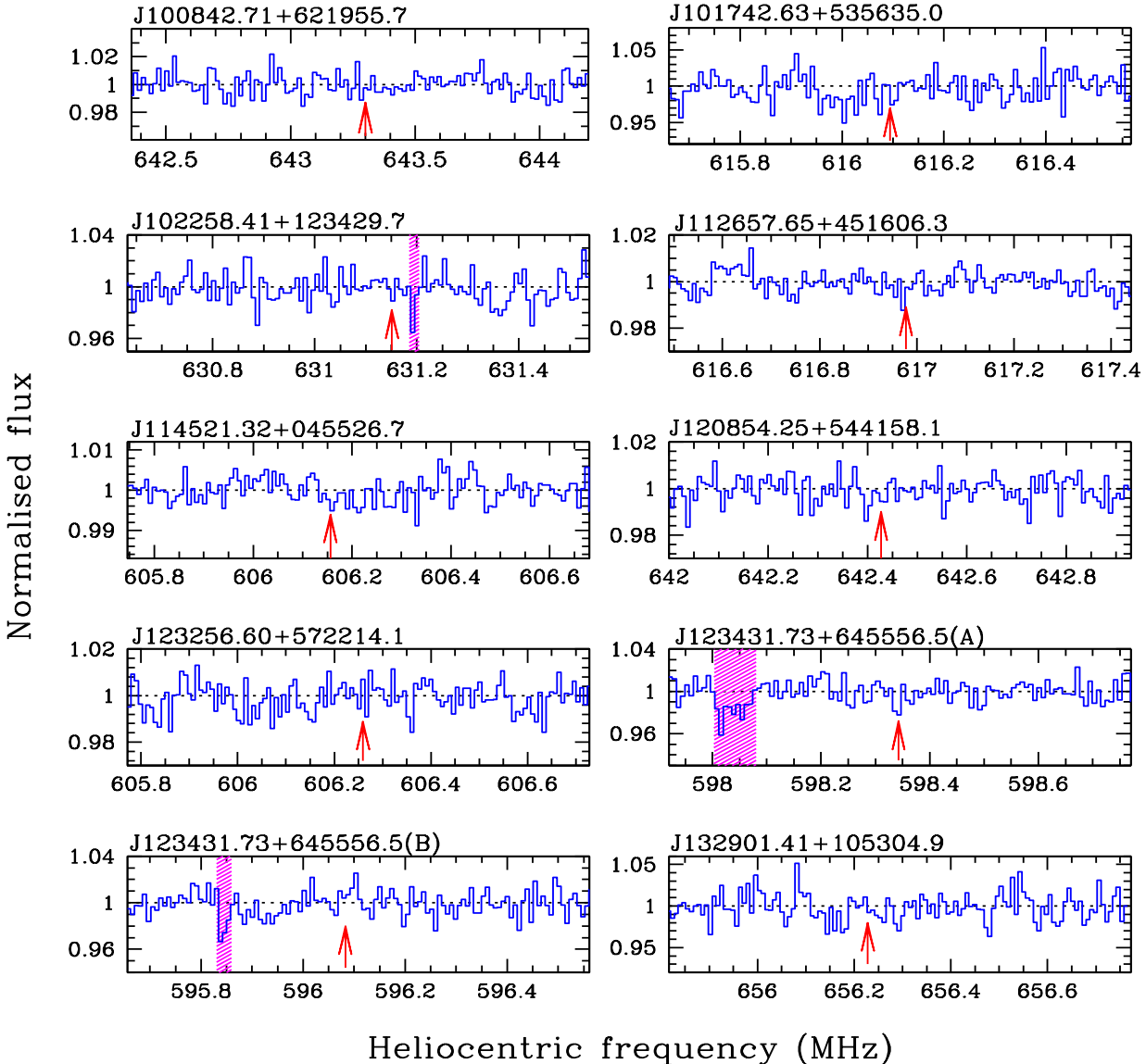
## 5 DETAILS OF NEW 21-CM ABSORBERS

In this Section, we give details on the nine 21-cm absorbers detected in our survey (Fig. 4). The total integrated 21-cm optical depths and velocity spreads of the absorption ( $\Delta V$ )

are listed in Table 4. We compute  $\Delta V$  using the apparent optical depth profile (see Fig. 6) and the method described by Ledoux et al. (2006). It is usual procedure to decompose the 21-cm absorption profile into multiple Gaussian functions. For a Gaussian profile  $N(\text{H I})$  and the peak optical depth ( $\tau_p$ ) are related by,

$$N(\text{HI}) = 1.93 \times 10^{18} \tau_p \frac{T_s}{f_c} \Delta v \text{ cm}^{-2}. \quad (2)$$

Here,  $\tau_p$ ,  $\Delta v$ , and  $f_c$  are the peak optical depth, the FWHM in  $\text{km s}^{-1}$  of the fitted Gaussian, and the covering factor of the absorbing cloud respectively. Individual Gaussian fits and fit parameters are presented in Fig. 4 and Table 4 respectively.

Figure 5. *Continued.*

In principle one can constrain the kinetic temperature  $T_K$  using the width of the absorption lines ( $T_K \leq 21.86 \times \Delta v^2$  K; e.g. Heiles & Troland 2003). However, FWHMs of individual Gaussian components fitted to the absorption profiles are generally broad and range from  $5 \text{ km s}^{-1}$  to  $100 \text{ km s}^{-1}$  when our resolution is  $\sim 4 \text{ km s}^{-1}$ . Most probably these line widths are dominated by processes other than simple thermal broadening and constraints on  $T_K$  are poor.

**J0108–0037:** The 21-cm absorption profile is well fitted with a single Gaussian function with  $\tau_p = 0.070 \pm 0.002$  and  $\Delta v = 16 \pm 1 \text{ km s}^{-1}$ . The absorption line width corresponds to an upper limit on the kinetic temperature of  $T_K \leq 5600 \text{ K}$ . Radio source J0108–0037 is resolved into two components separated by  $\sim 5 \text{ mas}$  ( $\sim 40 \text{ pc}$  at  $z_{\text{abs}} = 1.3710$ ) in the VLBA images at 2 and 8 GHz (Beasley et al. 2002). Of these two the strongest component contributes about 70% of the total flux. Since it is difficult to ascertain which of these compo-

nents is the radio core, estimate of  $f_c$  is highly uncertain. From the integrated optical depth given in Table 3, we derive  $N(\text{H I}) = 2.4 \times 10^{20} \text{ cm}^{-2}$  for  $f_c = 1$  and  $T_s = 100 \text{ K}$  (as in cold neutral medium (CNM) of the Galaxy (Kulkarni & Heiles 1988)). This is a lower limit on  $N(\text{H I})$  as  $f_c$  is most probably less than 1 and  $T_s$  could be larger than 100 K. Thus  $N(\text{H I})$  in the 21-cm component is consistent with this system being a DLA. The Zn II+CrII blend at  $\lambda = 2062 \text{ \AA}$ , the Si II and the Mn II absorption lines are clearly detected even in the low dispersion spectrum (see Fig. 7). As can be seen from Table 1, this system has  $W_r(\text{Mg II} \lambda 2796) \leq 0.5 \text{ \AA}$  and was observed in the early stages of the survey mainly because of the presence of strong absorption lines from weak metal transitions (see Fig. 7). For this reason this system will not figure in any analysis we perform using equivalent width limited samples.

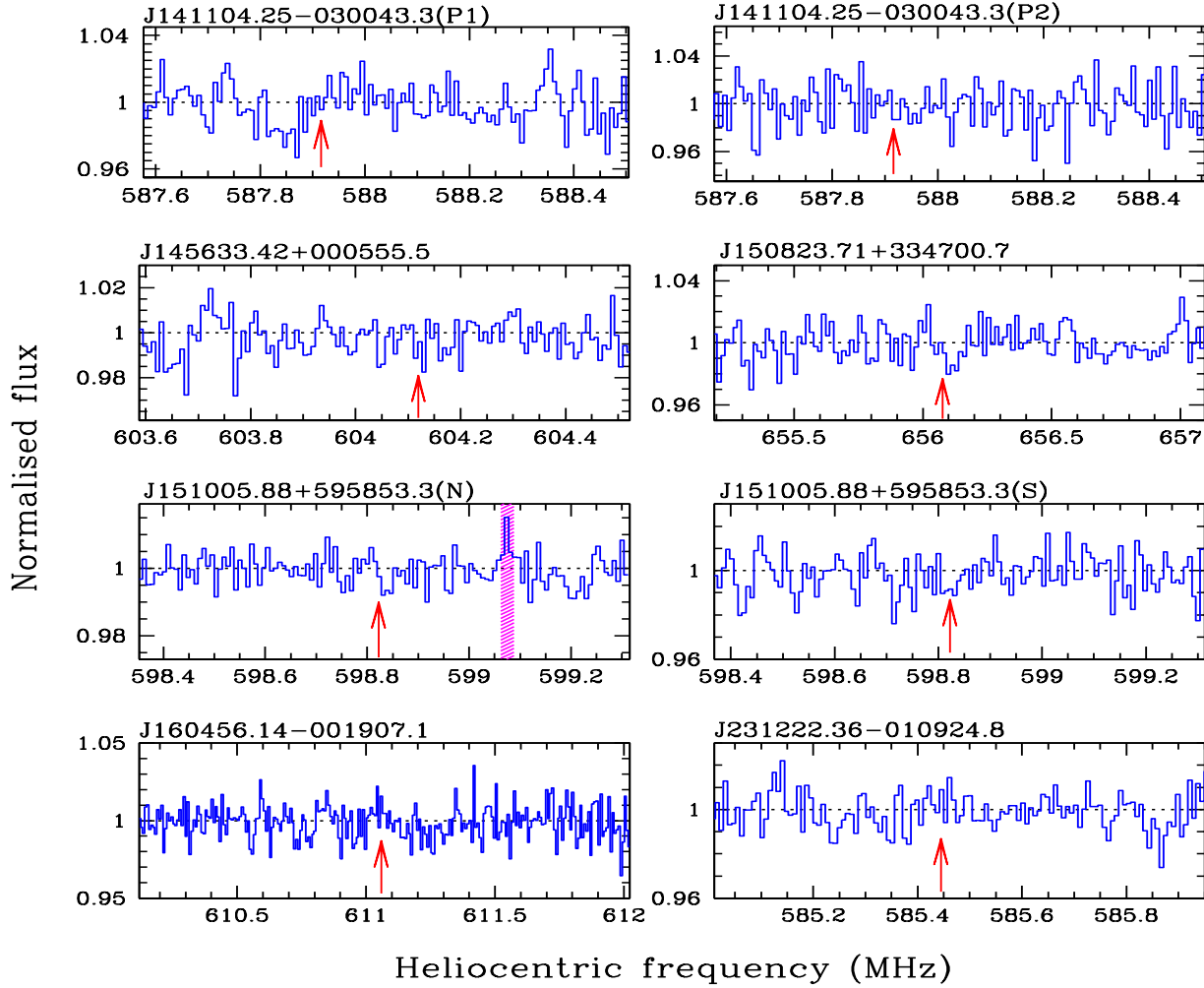
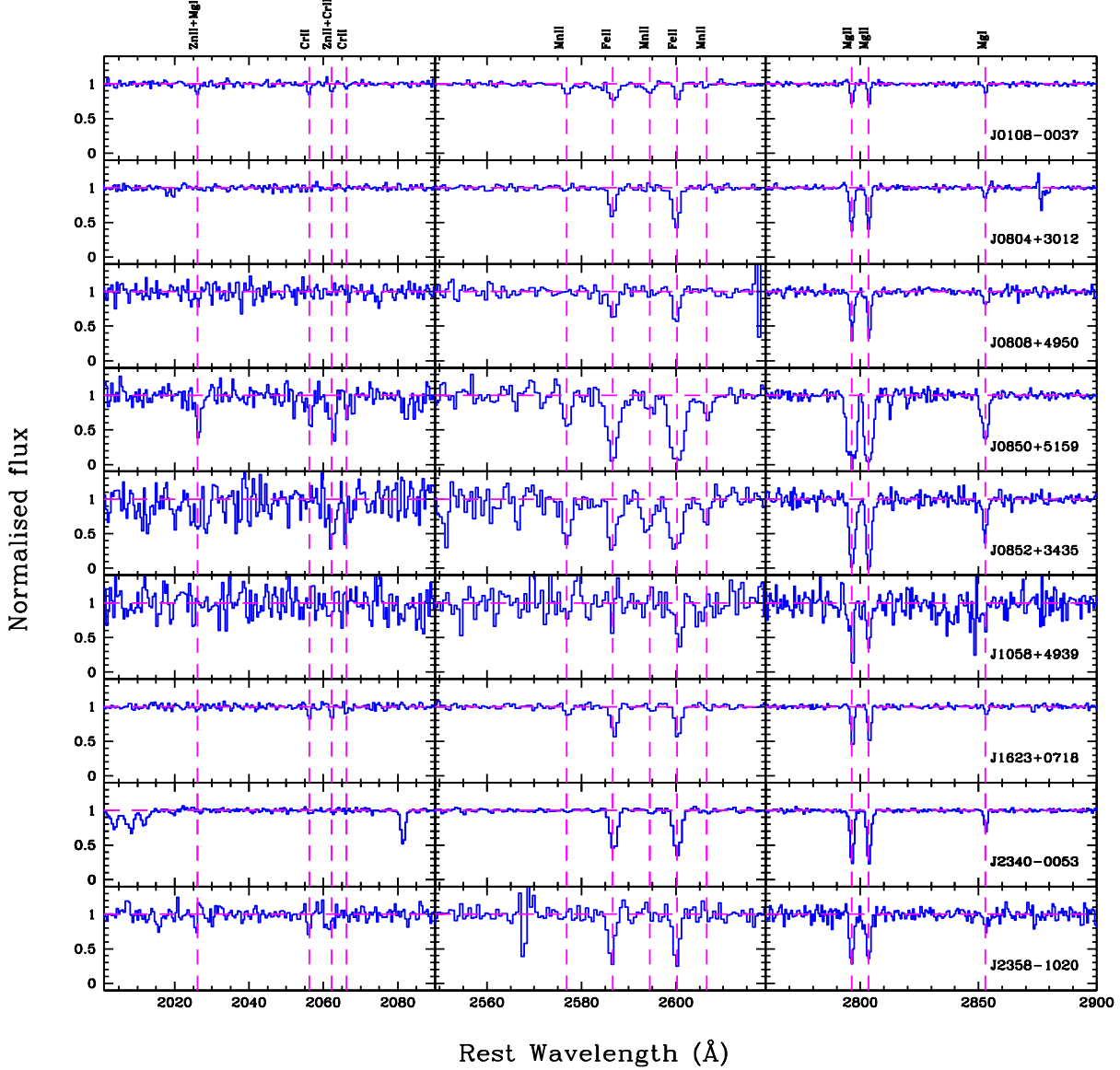
Figure 5. *Continued.*

Table 4. Characteristics of 21-cm absorption profiles and multiple Gaussian fits.

QSO	$\int \tau dv$	$\Delta V$	$\frac{f_c N(\mathrm{HI})^a}{T_s}$	$z_{\mathrm{abs}}$	$\Delta v^b$	$\tau_p^c$	$\frac{f_c N(\mathrm{HI})^d}{T_s}$
J0108-0037	1.29 $\pm$ 0.04	27.31	2.37 $\pm$ 0.07	1.37099	16 $\pm$ 1	0.070 $\pm$ 0.002	0.22 $\pm$ 0.02
J0804+3012	0.39 $\pm$ 0.03	130.1	0.72 $\pm$ 0.06	1.19069	86 $\pm$ 47	0.002 $\pm$ 0.001	0.03 $\pm$ 0.02
J0808+4950	0.10 $\pm$ 0.02	23.82	0.18 $\pm$ 0.04	1.40732	11 $\pm$ 2	0.008 $\pm$ 0.001	0.02 $\pm$ 0.01
J0850+5159	15.3 $\pm$ 0.5	61.38	28.1 $\pm$ 0.9	1.32674	49 $\pm$ 16	0.117 $\pm$ 0.036	1.11 $\pm$ 0.50
J0852+3435	6.91 $\pm$ 0.34	76.13	12.7 $\pm$ 0.6	1.30919	23 $\pm$ 7	0.347 $\pm$ 0.108	1.61 $\pm$ 0.57
J1058+4939	0.41 $\pm$ 0.04	32.85	0.75 $\pm$ 0.07	1.21168	26 $\pm$ 9	0.006 $\pm$ 0.001	0.03 $\pm$ 0.01
J1623+0718	0.91 $\pm$ 0.10	34.57	1.67 $\pm$ 0.18	1.33567	11 $\pm$ 2	0.042 $\pm$ 0.005	0.09 $\pm$ 0.02
J2340-0053	2.50 $\pm$ 0.24	7.76	4.59 $\pm$ 0.44	1.36087	2.5 $\pm$ 0.5	0.662 $\pm$ 0.207	0.32 $\pm$ 0.12
J2358-1020	0.23 $\pm$ 0.04	12.48	0.42 $\pm$ 0.07	1.17304	6 $\pm$ 1	0.183 $\pm$ 0.042	0.21 $\pm$ 0.11

<sup>a</sup> in units of  $10^{18} \mathrm{cm}^{-2}$ ; <sup>b</sup> FWHM in  $\mathrm{km} \mathrm{s}^{-1}$ ; <sup>c</sup> peak optical depth; <sup>d</sup> in units of  $10^{19} \mathrm{cm}^{-2}$



**Figure 7.** Normalised rest frame SDSS spectra of the Mg II systems with 21-cm detection. Vertical dashed lines mark the location of interesting metal line transitions.

**J0804+3012:** Broad and shallow 21-cm absorption detected towards this QSO was confirmed by observations at different epochs and using a wider baseband bandwidth of 2 MHz. Therefore, latter spectra have a factor 2 coarser velocity resolution (see Table 2). In Fig. 4, we show the weighted average of the spectra obtained after smoothing the spectrum of higher resolution. This system has the broadest velocity profile among the 21-cm absorbers in our sample. The overall absorption profile is fitted with a main component with  $\Delta v \sim 43 \text{ km s}^{-1}$  and a broad wing,  $\Delta v \sim 86 \text{ km s}^{-1}$ . Based on the integrated optical depth we derive  $N(\text{H I}) = 7.0 \times 10^{17} (T_s/f_c) \text{ cm}^{-2}$ .

This source is resolved into three components in the MERLIN images obtained at 1.6 GHz and 5 GHz with angular resolutions  $0.178'' \times 0.155''$  and  $0.073'' \times 0.037''$  respectively (Kunert et al. 2002). The angular extent of the radio

emission in these images is  $\sim 1.4''$  with 77% of the flux contributed by the central component. However, at 1.4 GHz these three components account for only 50% of the flux measured in FIRST images. The structure of the source is thus highly complex. This could very well explain the large velocity spread of the 21-cm absorption. This source is ideal for VLBA spectroscopy to study the internal structure of the intervening Mg II system. Apart from Mg II, Fe II and Mg I absorption lines no other metal absorption lines are detected in the SDSS spectrum (see Fig. 7).

**J0808+4950:** The background QSO at  $z_{\text{em}} = 1.432$  is classified as highly polarized Blazar/QSO with radio components at mas scales showing superluminal motion (see Piner et al. 2007). The measured apparent velocity is  $v_a \sim 15c$  with  $c$  being the speed of light. This source is also known to show strong flux variability at high radio frequencies (Teras-

**Table 2.** Observing log for the GMRT observations.

Source name	$z_{\text{abs}}$	Date	Time (hr)	Ch. Width (km s $^{-1}$ )	
(1)	(2)	(3)	(4)	(5)	
J0108-0037	1.3710	2007 Jul 03	4.4	3.9	
J0154-0007	1.1803	2007 Jan 30	5.3	3.6	
J0214+1405	1.4463	2006 Jul 16	4.4	4.0	
J0240-2309	1.3647	2004 Feb 09	8.0	3.9	
J0259-0019	1.3370	2006 Oct 06	2.3	3.9	
J0742+3944	1.1485	2007 Dec 31	6.3	3.5	
J0748+3006	1.4470	2006 Aug 01	5.5	4.0	
J0802+2917	1.3648	2007 Nov 26	7.0	3.9	
J0804+3012	1.1908	2006 Aug 22	6.0	3.6	
		2006 Sep 15,16	6.2	7.2 <sup>2,128</sup>	
J0808+4950	1.4071	2006 Dec 06	5.3	4.0	
		2008 May 08	5.1	4.0	
J0812+2522	1.3683	2007 Feb 01	5.8	3.9	
J0845+4257	1.1147	2006 Sep 09	5.0	3.5	
J0850+5159	1.3265	2007 Nov 06	7.3	3.8	
J0852+3435	1.3095	2007 Nov 05	7.5	3.8	
		2007 Nov 30	6.9	3.8	
		2008 Mar 08	6.2	3.8	
J0953+3225	1.2372	2007 Jun 05	5.8	3.7	
J1008+6219	1.2080	2006 Oct 06	6.5	3.6	
J1017+5356	1.3055	2006 Aug 29	4.4	3.8	
J1022+1234	1.2505	2007 Nov 29	8.3	3.7	
J1058+4939	1.2120	2008 May 10	5.9	3.6	
J1126+4516	1.3022	2007 Dec 29	5.5	3.8	
J1145+0455	1.3433	2007 Jan 30	5.2	3.9	
J1208+5441	1.2110	2008 May 11	6.1	3.7	
J1232+5722	1.3429	2007 Dec 28	5.6	3.9	
J1234+6455	1.3739	2008 Jan 02	5.6	3.9	
		1.3829	2007 Dec 30	5.4	3.9
J1329+1053	1.1645	2007 Jun 21	5.2	3.6	
J1411-0300	1.4160	2006 Jul 06,07	3.9	4.0	
J1456+0005	1.3512	2008 Jan 01	6.1	3.9	
J1508+3347	1.1650	2007 Jun 05	4.1	3.6	
J1510+5958	1.3720	2007 Feb 02	5.6	3.9	
J1604-0019	1.3245	2006 Jun 19	3.3	3.8 <sup>2,256</sup>	
J1623+0718	1.3350	2007 Dec 16	5.4	3.9	
		2008 May 09	6.3	3.9	
J2312-0109	1.4262	2006 Oct 04	4.3	4.0	
J2340-0053	1.3603	2007 Jan 21	5.8	3.9	
		2007 Apr 03	5.8	1.0 <sup>0.25,128</sup>	
J2358-1020	1.1726	2006 May 23	3.9	3.6	
		2006 Jul 30	5.5	1.8 <sup>0.5,128</sup>	

Col. 1: Source name; col. 2: Mg II absorption redshift; col. 3: Date of observation; col. 4: Time on source; col. 5: Channel width in km s $^{-1}$ . Superscripts to channel width give the baseband bandwidth in MHz and number of spectra channels for the observation when a baseband set-up different from 1 MHz split into 128 channels was used.

ranta et al. 2005). We detect a weak 21-cm absorption towards this quasar with absorption redshift  $z_{\text{abs}}=1.407$ , only  $\sim 3000$  km s $^{-1}$  away from the QSO emission redshift. Absorption was confirmed by repeated observations at epochs separated by seven months. We do not note any strong flux variation between these observations. The spectrum presented in Fig. 4 results from the combination of all data. The absorption profile is well fitted with a single Gaussian component with  $\tau_p=0.008\pm 0.001$  and  $\Delta v=11\pm 2$  km s $^{-1}$ .

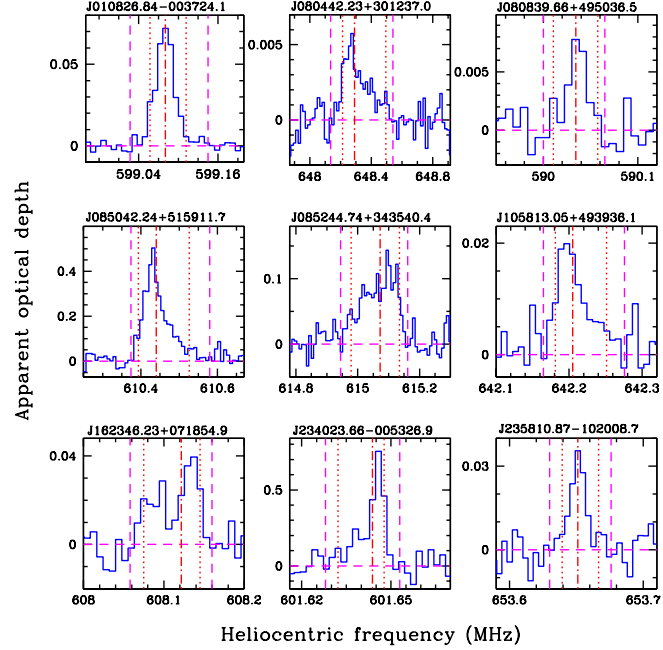


**Figure 6.** Apparent optical depth of 21-cm absorption features detected in our GMRT survey. The outermost dashed vertical lines give the velocity range over which the optical depth is integrated. The dotted vertical lines correspond to the width of the profile minus 5% of the absorption on both sides (see Fig. 1 of Ledoux et al. 2006).

This source is unresolved at 8 GHz from MERLIN observations part of the CLASS/JVAS survey with a beam size of  $0.227''\times 0.203''$ . VLBA observations at 2 and 8 GHz resolve the source into two components with a separation of 2 and 1 mas respectively (Fey & Charlot 2000). The strongest component accounts for 85% of the flux detected in the VLBA map. However the total flux density 480 mJy measured at 8 GHz in the VLBA observations accounts only for 55% of the flux detected in the MERLIN image. It is not clear whether this difference is due to flux variations or to a considerable fraction of the flux being emitted in a diffuse component that is resolved in the VLBA images. The H I column density derived from our GMRT observations is,  $N(\text{H I})=2.2\times 10^{19}(T_s/100)(0.85/f_c)\text{ cm}^{-2}$ . Only Mg II, Fe II and Mg I absorptions are detected in the SDSS spectrum (See Fig. 7).

**J0850+5159:** Radio source J0850+5159 is compact at mas scales in the VLBA images at 5 and 15 GHz (Taylor et al. 2005) implying  $f_c \sim 1.0$ . Strong ( $\tau_p=0.50$ ) 21-cm absorption is detected towards this QSO which is extremely red at optical and NIR wavelengths (u-K $\sim 4.8$  mag). The total 21-cm H I column density, with  $f_c = 1$ , is  $N(\text{H I}) = (2.81\pm 0.09)\times 10^{19} T_s \text{ cm}^{-2}$ . Numerous absorption lines are detected in the SDSS spectrum in addition to Mg II, Fe II and Mg I (see Fig. 7). A 2175 Å feature is also present at  $2.7\sigma$  significance level at the redshift of the intervening Mg II system (Srianand et al. 2008b). An independent estimate of  $N(\text{H I})$  was derived by fitting a LMC2 extinction curve to the QSO spectrum,  $N(\text{H I}) = 5.73\pm 1.10\times 10^{21} \text{ cm}^{-2}$ . Therefore we conclude that  $T_s \sim 204 \pm 40$  K (see Srianand et al. 2008b for more details).

**J0852+3435:** Broad and shallow 21-cm absorption, confirmed by observations at three different epochs, is detected towards this red QSO (u-K $\sim$ 5.6 mag). Details about the 2175 Å feature detected at  $> 5\sigma$  significance level at the redshift of the Mg II absorption system are presented in Srianand et al. (2008b). Numerous absorption lines are detected in the SDSS spectrum in addition to Mg II, Fe II and Mg I (see Fig. 7). The background radio source is compact in CLASS/JVAS and has flat radio spectrum (Jackson et al. 2007). Total 21-cm H I column density with  $f_c = 1$  is,  $N(\text{H I}) = (1.27 \pm 0.06) \times 10^{19} T_s \text{ cm}^{-2}$ . An independent estimate of  $N(\text{H I})$  was derived by fitting the LMC2 extinction curve to the QSO spectrum  $N(\text{H I}) = 6.97 \pm 1.30 \times 10^{21} \text{ cm}^{-2}$ . Therefore we conclude that  $T_s \sim 550 \pm 106 \text{ K}$  (Srianand et al. 2008b).<sup>2</sup>

**J1058+4939:** The 21-cm absorption line detected towards this QSO is fitted well with two Gaussian components. The radio source is unresolved in the FIRST and GMRT images. The quasar is known to show variability at 151 MHz. Riley & Warner (1994) found that roughly 60% of the total flux at 5 and 8 GHz comes from a region smaller than  $\leq 0.1''$  implying  $f_c = 0.6$ . VLBA or MERLIN images are not available for this source. Integrated 21-cm optical depth yields  $N(\text{H I}) = 1.25 \times 10^{20} (T_s/100)(0.6/f_c) \text{ cm}^{-2}$ . The SNR of the SDSS spectrum is poor and only a few absorption lines are detected (see Fig. 7).

**J1623+0718:** 21-cm absorption is detected in two well detached components. The background radio source is unresolved in GMRT and FIRST images. The source is compact even in CLASS/JVAS and has a flat radio spectrum (Jackson et al. 2007). Thus  $f_c$  could be close to 1 at  $\sim 100$  mas scales. The integrated 21-cm optical depth yields  $N(\text{H I}) = 1.7 \times 10^{18} T_s \text{ cm}^{-2}$ . The Zn II+Cr II blend at  $\lambda=2062$  Å, the Si II and the Mn II absorption lines are clearly detected even in the SDSS low dispersion spectrum (see Fig. 7).

**J2340–0053:** Radio source J2340–0053 is compact at mas scales in VLBA observations at 2 and 8 GHz (Kovalev et al. 2007). The 21-cm absorption is narrow and the spectrum presented in Fig. 4 was obtained with a resolution of  $1.0 \text{ km s}^{-1}$  per channel. The main component has a FWHM of  $2.5 \pm 0.5 \text{ km s}^{-1}$  which corresponds to an upper limit of 136 K for the kinetic temperature. Clearly the gas responsible for this system is cold. It is most likely that  $f_c \sim 1$  for this system. Under the assumption that  $f_c = 1$  and  $T < 200$  K, we derive  $N(\text{H I}) \leq 9 \times 10^{19} \text{ cm}^{-2}$ . This means the component responsible for this 21-cm absorption is most probably a sub-DLA. An optical spectrum of this QSO was analysed by Khare et al. (2004). In Fig. 8 we show absorption lines associated to this systems on a velocity scale. The corresponding high spectral resolution KECK spectrum was obtained by Prochaska et al. (2007). The vertical dashed lines mark the location of the 21-cm absorption. It is clear that the 21-cm absorption is not originating from the component that dominates the equivalent width of strong metal lines.

<sup>2</sup> Note errors in  $T_s$  measurements for this system and the system at  $z_{\text{abs}} = 1.326$  towards J0850+5159 are slightly reduced compared to that given in Srianand et al. (2008b) because of different procedures (we use here the errors obtained from the apparent optical depth profile technique).

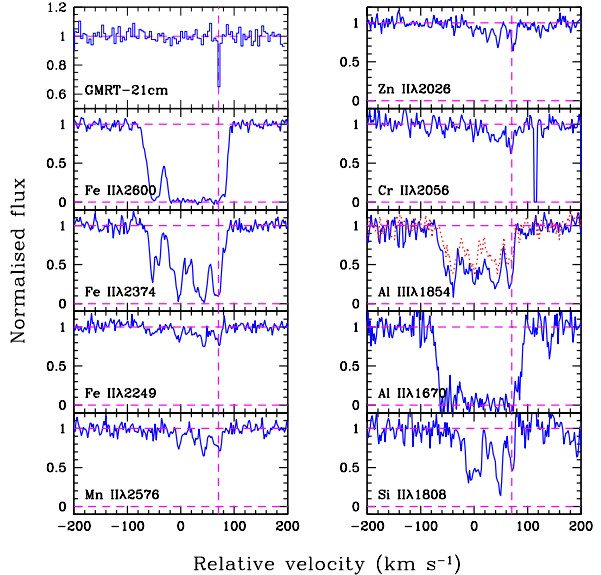


**Figure 8.** Absorption lines in the  $z_{\text{abs}} = 1.3609$  system towards J2340–0053 observed at high spectral resolution (Prochaska et al. 2007). The dotted line spectrum corresponds to Al III $\lambda 1862$ . Dashed vertical lines show the location of the 21-cm absorption line.

Weak metal lines such as Fe II $\lambda 2249$  suggest that  $\sim 30\%$  of the metals are in this component. The compactness of the background quasar and the fact that the metal absorption component associated with 21-cm is well detached from the central blend makes it an interesting system for measuring the time evolution of fundamental constants. However, the publicly available KECK data is not sufficient for this purpose.

**J2358–1020:** The background radio source is unresolved in high frequency VLBA observations (Fomalont et al. 2000; Fey & Charlot, 2000) and  $f_c$  could be close to unity. The absorption profile is well fitted with a single Gaussian component whose FWHM implies a kinetic temperature  $\leq 800$  K. This gives  $\log[N(\text{H I})] \leq 20.5$  for  $f_c = 1$ . The Zn II+Cr II $\lambda 2062$  Å blend is clearly detected in the low dispersion SDSS spectrum (Fig. 7).

## 6 DETECTABILITY OF 21-CM ABSORPTION

In this Section, we investigate the relationship between the detectability of 21-cm absorption and properties of UV absorption lines from the Mg II systems. This may help in particular to preselect more efficiently candidates for future 21-cm surveys.

### 6.1 Rest equivalent width of Mg II absorption

First we concentrate on  $W_r(\text{Mg II}\lambda 2796)$ , the only quantity that has been used to define our present sample. In panel (a) of Fig. 9 we plot  $W_r(\text{Mg II}\lambda 2796)$  against the integrated 21-cm optical depth for all the systems in our GMRT sample. Detections (resp. non detections) are marked by filled (resp. open) circles. Even though the system with strongest

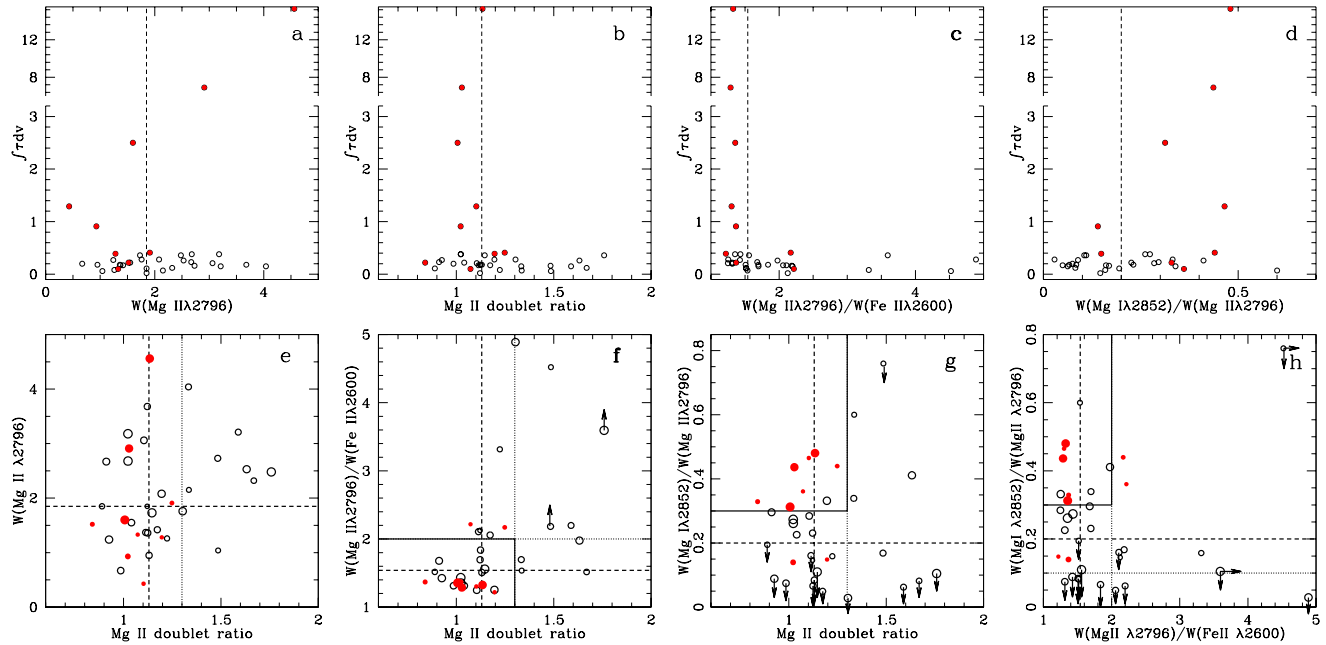


**Figure 9.** Top panels: The integrated 21-cm optical depth is plotted against various parameters of the UV absorption lines derived from the SDSS spectra. In the case of detection (filled circle) the optical depth is obtained by integrating over the observed absorption profile. Open circles are for 21-cm non-detections in which case limits are obtained by integrating the optical depth over a Gaussian component with peak optical depth corresponding to the  $3\sigma$  rms limit in the continuum and width  $10 \text{ km s}^{-1}$ . Bottom panels: Different parameters of UV absorption lines are plotted against one another. Symbols are as in upper panels. The size of the symbols are scaled by the 21-cm optical depth limits (per  $10 \text{ km s}^{-1}$ ) reached. The vertical dashed line in all the panels gives the median value. Other lines indicate the limiting values and/or allowed ranges as discussed in the text.

21-cm absorption in our sample has the largest equivalent width, we do not find evidence for a correlation between the two quantities. Indeed, the median  $W_r(\text{Mg II} \lambda 2796)$  is  $1.85 \text{ \AA}$  for the systems observed with GMRT and there are only three (out of 9) 21-cm detections from systems having  $W_r(\text{Mg II} \lambda 2796) \geq 1.85 \text{ \AA}$ . As we have reached similar limiting 21-cm optical depth over the whole range of  $W_r(\text{Mg II} \lambda 2796)$  sampled by our survey, this can not be due to any artifact introduced by variation of the optical depth limits through the sample.

For comparison with our sample, we summarize in Table 6 the properties of systems with  $W_r(\text{Mg II} \lambda 2796) \geq 1 \text{ \AA}$  in the low- $z$  sample of Lane (2000). The median  $W_r(\text{Mg II} \lambda 2796)$  and redshift in this subsample is  $1.75 \text{ \AA}$  and  $z_{\text{abs}}=0.7$ . There are 2 and 5 detections respectively in systems with  $W_r(\text{Mg II} \lambda 2796)$  below and above the median value. It seems therefore that the probability to detect 21-cm absorption in strong Mg II systems is higher at lower redshift. We further investigate this issue in the next Section.

## 6.2 Mg II Doublet ratio (DR)

In panel (b) of Fig. 9 we plot the integrated 21-cm optical depth vs. the Mg II doublet ratio (DR). It is clear that 21-cm detected systems are confined to regions with  $DR < 1.3$ . For the systems with  $W_r(\text{Mg II} \lambda 2796) \geq 1 \text{ \AA}$  and  $DR < 1.3$  we detect 21-cm absorption in roughly  $33^{+17\%}_{-12\%}$  (8/24) of the systems to be compared to the overall success rate in the sample,  $24^{+12\%}_{-8\%}$  (8/33). The median value of DR in our

sample is 1.12 and only two systems with DR greater than this are detected in 21-cm absorption.

As pointed out by Petitjean & Bergeron (1990) the number of Voigt profile components found in high resolution spectra correlates well with the total equivalent width of blended lines (see Fig. 3 of Ellison 2006). Thus equivalent widths measured in SDSS data reflect primarily the number of individual components and/or the velocity spread between them and not directly the column density (see P06). On the contrary, a doublet ratio close to 1, even in a low dispersion spectrum, means high level of saturation and therefore high column density. Thus systems with high  $W_r(\text{Mg II} \lambda 2796)$  and  $DR \sim 1$  provide higher probability of a line of sight hitting high Mg II column density clouds.

Interestingly, in the GMRT sample, there are 9 systems with  $DR > 1.3$  and 7 of these systems have  $W_r(\text{Mg II} \lambda 2796) > 1.85 \text{ \AA}$  (see panel e of Fig. 9). The lower detection rate of 21-cm absorption in systems with  $W_r(\text{Mg II} \lambda 2796) > 1.85$  in the GMRT sample could be due to high values of DR in most of these systems. It is most likely that the high value of  $W_r(\text{Mg II})$  in these systems is primarily due to the velocity field and not to a large Mg II column density.

From Fig. 3.3 of Lane (2000) we find that all the low- $z$  21-cm detections have  $DR \leq 1.4$ . Thus our finding of high detection rate of 21-cm absorption in systems with low DR is consistent with what is seen for low- $z$  21-cm absorbers. The difference between high and low redshift sample noted in the previous Section is therefore probably related to a redshift evolution in the overall structure of Mg II systems.

### 6.3 The $W_r(\text{Mg II}\lambda 2796)/W_r(\text{Fe II}\lambda 2600)$ ratio

RTN06 showed that DLAs have  $1.0 \leq W_r(\text{Mg II}\lambda 2796)/W_r(\text{Fe II}\lambda 2600) \leq 2$ . We shall call this ratio  $R_1$ . In their Mg II sample there are 19 systems in the redshift range  $1.10 \leq z \leq 1.45$ , with  $W_r(\text{Mg II}\lambda 2796) \geq 1\text{\AA}$  and  $R_1$  in the above mentioned range. Seven of them (i.e  $37_{-14}^{+20}\%$ ) have  $\log N(\text{H I}) \geq 20.3$  and are DLAs as per the conventional definition. However, 18 of these 19 systems have  $\log N(\text{H I}) \geq 19.6$ .

From Panel (c) of Fig 9 it is clear that our selection of systems based on  $W_r(\text{Mg II}\lambda 2796)$  alone has ensured that a large fraction of systems (24/33) in our sample have  $R_1$  in the above mentioned range. In addition, the detection rate of 21-cm absorption in our sample is high when  $R_1$  is low. The median value of  $R_1$  in our sample is 1.54. About  $41_{-15}^{+22}\%$  (resp.  $11_{-7}^{+15}\%$ ) of the systems with  $R_1 < 1.54$  (resp.  $> 1.54$ ) show 21-cm absorption. In the  $R_1$  range covered by DLAs in RTN06 we find that there are 24 Mg II systems in our sample with 7 of them (i.e  $29_{-11}^{+16}\%$ ) showing detectable 21-cm absorption. The other two detections have  $R_1$  consistent with 2 within measurement uncertainties. For comparison, in the low- $z$  sample of Lane (2000) there are 11 systems with  $1 \leq R_1 \leq 2$  and 6 of them show 21-cm absorption.

In panel (f) of Fig. 9 we plot  $R_1$  vs DR. Out of the 20 systems with both  $DR < 1.3$  and  $R_1 < 2$ , 7 systems show 21-cm absorption (i.e  $35_{-13}^{+19}\%$ ) systems. This is very close to the detection rate we obtained with the condition  $DR < 1.3$  only. Reducing the upper limit of  $R_1$  to 1.6 produces an increase of the detection rate to  $41_{-15}^{+22}\%$ .

Finally we notice that roughly half the systems with  $W_r(\text{Mg II}\lambda 2796) > 1.85\text{\AA}$  also have  $R_1 > 2$ . This again suggests that in this redshift range large  $W_r(\text{Mg II}\lambda 2796)$  does not guarantee high column density.

### 6.4 The $W_r(\text{Mg I}\lambda 2852)/W_r(\text{Mg II}\lambda 2796)$ ratio

From the data listed in Table 1 of RTN06 we find that the DLA population with  $W_r(\text{Mg II}\lambda 2796) \geq 1\text{\AA}$  has  $W_r(\text{Mg I}\lambda 2852)/W_r(\text{Mg II}\lambda 2798)$  (called  $R_2$  from now on) in the range 0.01 to 0.6. Conversely,  $\sim 30_{-6}^{+7}\%$  of systems with  $0.01 < R_2 < 0.6$  are DLAs. The fraction increases to  $\sim 52_{-14}^{+19}\%$  for  $R_2 > 0.3$ . In addition,  $92_{-19}^{+8}\%$  of the systems with  $R_2 > 0.3$  have  $\log N(\text{H I}) > 19.60$ . From the sample of Lane (2000) we find that 35% (resp. 40%) of the systems with  $W_r(\text{Mg II}\lambda 2796) > 1\text{\AA}$  and  $R_2 > 0.1$  (resp.  $R_2 > 0.3$ ) show detectable 21-cm absorption. Note however that the Mg I $\lambda 2852$  equivalent width is not always available.

It is clear from panel (d) of Fig. 9 that all our 21-cm detections, in consistency with the results from low-redshift studies, are associated with  $R_2 > 0.1$ . We find that the detection rate of 21-cm absorption is  $\sim 36_{-12}^{+16}\%$  when  $R_2 > 0.1$ . About  $44_{-16}^{+24}\%$  of the systems with  $R_2 > 0.2$  (the median value in our sample) show 21-cm absorption. If we restrict ourselves to  $R_2 > 0.3$  the detection rate in our sample increases to  $70_{-26}^{+30}\%$ . It is also apparent from panel (g) of Fig 9 that a joint constraint,  $DR < 1.3$  and  $R_2 > 0.3$  (solid box in this panel), gives a  $88_{-31}^{+12}\%$  detection rate (7 out of 8) for 21-cm absorption. Thus it appears that using joint constraints on DR and  $R_2$  can yield a very high detection rate of 21-cm absorption. This is confirmed by the low- $z$  data of Lane(2000) summarized in Table 6. There are only 5 systems (exclud-

**Table 5.** Sample of sources with milli-arcsecond scale images

QSO	$f_c$ (VLBA)	LAS (mas)	$W_r(\text{Mg II}\lambda 2796)$ (\text{\AA})	$\frac{1}{f_c} \int \tau dv$ (km s $^{-1}$ )
(1)	(2)	(3)	(4)	(5)
J0108-0037	0.30–0.70 <sup>1</sup>	5.5	$0.43 \pm 0.05$	1.84–4.3
J0240-2309	0.65 <sup>2</sup>	10.0	$1.85 \pm 0.002$	$\leq 0.03$
J0259-0019	1.00 <sup>1</sup>	$\leq 15$	$1.76 \pm 0.04$	$\leq 0.28$
J0742+3944	0.58 <sup>3</sup>	8.1	$2.48 \pm 0.41$	$\leq 0.62$
J0748+3006	0.41 <sup>3</sup>	54.3	$3.68 \pm 0.06$	$\leq 0.44$
J0808+4950	0.85 <sup>3</sup>	9.7	$1.33 \pm 0.09$	0.12
J0850+5159	0.99 <sup>3</sup>	3.0	$4.56 \pm 0.12$	15.5
J0953+3225	0.84 <sup>3</sup>	3.2	$1.55 \pm 0.05$	$\leq 0.26$
J1126+4516	0.57 <sup>3</sup>	5.6	$1.26 \pm 0.25$	$\leq 0.14$
J1208+5441	0.88 <sup>3</sup>	1.2	$1.85 \pm 0.25$	$\leq 0.13$
J1508+3347	0.74 <sup>3</sup>	11.4	$2.67 \pm 0.08$	$\leq 0.31$
J2340-0053	0.87 <sup>4</sup>	13.6	$1.60 \pm 0.04$	2.87
J2358-1020	0.98 <sup>2</sup>	2.2	$1.52 \pm 0.15$	0.24

<sup>1</sup> Beasley et al. 2002 (2 & 8 GHz); <sup>2</sup> Fomalont et al. 2000 (5 GHz); <sup>3</sup> Helmboldt et al. 2007 (5 GHz); <sup>4</sup> Kovalev et al. 2007 (2 & 8 GHz)

ing poor upper limits on Mg I) with  $R_2 > 0.3$  and 3 of them show detectable 21-cm absorption. One of these non-detections ( $z_{\text{abs}} = 0.9004$  towards 1629+120) has  $DR = 1.6$  and the other system ( $z_{\text{abs}} = 0.7713$  towards 1556–245) has  $R_1 > 5$ .

From panel (h) of Fig. 9, it can be seen that joint constraints on  $R_1$  and  $R_2$  does not produce higher detection rate compared to that obtained from the joint constraints on DR and  $R_1$ .

### 6.5 Milliarcsecond scale radio structure

We address here possible effects introduced by issues related to covering factor of the background source that may play an important role on the detectability of 21-cm absorption. Although VLBI spectroscopy at 467 MHz of the  $z_{\text{abs}} = 2.04$  DLA towards PKS 0458-020 suggests that the absorbing gas covers a large fraction of the extended ( $\geq 17$  kpc) radio components (Briggs et al. 1989), time-variability of 21-cm optical depth seen in the absorbers towards B0235+164 and B1127–145 suggest that absorbing gas is patchy at sub-kpc scales (Wolfe, Briggs & Davis, 1982; Kanekar & Chengalur, 2001). In addition, spatially resolved spectroscopy of the three closely spaced ( $< 1$  arcsec) images of APM 0827+5255 have revealed a strong variation in Mg II optical depths over kpc scales (Petitjean et al. 2000; Ellison et al. 2004).

At present, low frequency (i.e  $< 1.4$  GHz) mas scale images are not available for any of the sources in our sample. Our ongoing VLBA observations at low frequencies will provide better constraints on  $f_c$  in the near future. However, high frequency (i.e  $\geq 2$  GHz) milli-arcsecond scale images are available for 13 sources out of the 22 sources that are compact in FIRST and our 610 MHz images. We give details of these objects in Table 5. Measured covering fraction ( $f_c$ ) and largest angular size (LAS) are given in columns 2 and 3 respectively. Covering fraction has been estimated as the ratio of the core flux density to the total flux density detected in the VLBA images. To achieve as much uniformity as pos-

**Table 6.** Sample of Mg II systems with  $W_r(\text{Mg II}\lambda 2796) \geq 1 \text{ \AA}$  from Lane (2000).

Source name	$z_{\text{em}}$	$z_{\text{abs}}$	$W_r(\text{Mg II}\lambda 2796)$ (\text{\AA})	$W_r(\text{Mg II}\lambda 2803)$ (\text{\AA})	$W_r(\text{Mg I}\lambda 2852)$ (\text{\AA})	$W_r(\text{Fe II}\lambda 2600)$ (\text{\AA})	$\text{dv}$ ( $\text{km s}^{-1}$ )	$\tau_{3\sigma}$	$\int \tau \text{dv}$ ( $\text{km s}^{-1}$ )
(1)	(2)	(3)	(4)	(5)	(6)	(7)	(8)	(9)	(10)
0109+176	2.155	0.8392	1.75	1.20	<0.20	1.09	9.1	0.108	<1.09
0109+200	0.746	0.5346	2.26	1.71	....	....	7.6	0.029	<0.27
0229+341	1.240	0.7754	1.92	2.02	<1.13	....	8.8	0.043	<0.43
0235+164	0.940	0.5238	2.42	2.34	0.91	1.79	1.6 <sup>\ddagger</sup>	0.007	13.0
0248+430	1.316	0.3939	1.86	1.42	0.70	1.03	5.8	0.032	2.99
0420-014	0.915	0.6330	1.02	0.86	<0.36	....	10.6	0.146	<1.59
0454+039	1.343	0.8597	1.53	1.40	0.37	1.11	10.0	0.010	<0.11
0735+178 <sup>\dagger</sup>		0.4246	1.33	1.04	0.18	0.87	3.5	0.058	<0.36
0827+243	0.939	0.524	2.90	2.20	....	1.90	10.0 <sup>*</sup>	0.004	0.22
0805+046	2.876	0.9598	1.01	0.83	<0.60	0.24	4.9	0.095	<0.71
0957+003	0.907	0.6720	1.77	1.32	....	....	8.3	0.105	<0.01
1127-145	1.187	0.3130	2.21	1.90	1.14	1.14	5.4	0.021	3.11
1218+339	1.519	0.7423	1.34	1.08	<0.70	1.00	8.6	0.020	<0.20
1229-021	1.038	0.3950	2.22	1.93	0.49	1.59	1.0 <sup>\ddagger</sup>	0.007	3.00
1327-206	1.169	0.8530	2.11	1.48	<0.40	0.76	9.2	0.201	<2.04
1354+258	2.004	0.8585	1.00	0.86	<0.10	<0.20	9.2	0.103	<1.05
1556-245	2.815	0.7713	2.07	1.91	1.07	<0.20	8.8	0.068	<0.68
1622+238	0.927	0.6560	1.29	<1.69	<0.40	1.13	10.0 <sup>\ddagger</sup>	0.004	2.20
1629+120	1.795	0.5313	1.40	1.35	0.31	0.70	0.6 <sup>*</sup>	0.004	0.49
"	0.9004		1.06	0.67	0.44	0.63	9.4	0.080	<0.82
2212-299	2.703	0.6329	1.26	1.00	0.36	....	8.1	0.217	<2.07

Col. 1: source name as given in Lane (2000); col. 2: QSO emission redshift; col. 3: Absorption redshift of Mg II system; cols. 4, 5, 6 and 7: Rest equivalent widths of Mg II $\lambda 2796$ , Mg II $\lambda 2803$ , Mg I $\lambda 2852$  and Fe II $\lambda 2600$ ; cols. 8 and 9: spectral resolution and  $3\sigma$  uncertainty on the optical depth; col. 10: integrated 21-cm optical depth for the detections or  $3\sigma$  upper limit to it in case of non-detections. The upper limits on  $\int \tau \text{dv}$  have been computed for  $\text{dv}=10 \text{ km s}^{-1}$ .

<sup>\dagger</sup> BL Lacertae object a featureless continuum except for the intervening absorption line system at  $z_{\text{abs}}=0.4246$  (Carswell et al. 1974).

<sup>\ddagger</sup> 21-cm absorption data for 0235+164, 1229-021 and 1622+238 are originally from Wolfe et al. (1978), Brown & Spencer (1979) and Curran et al. (2007) respectively.

\* 21-cm absorption data for 0827+243 and 1629+120 are from Kanekar et al. (2003).

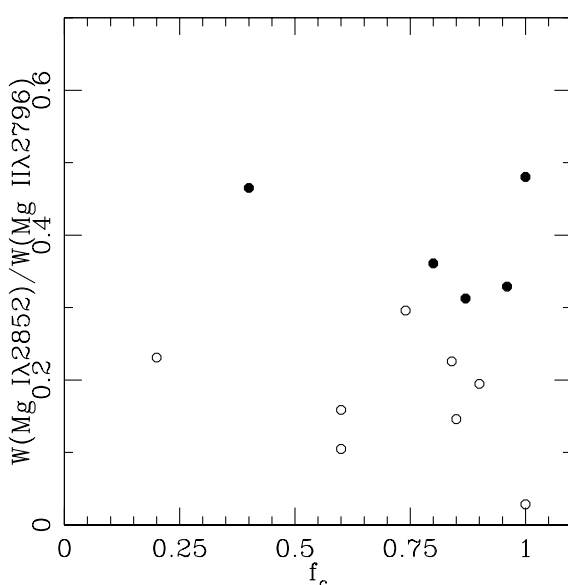


**Figure 10.** The ratio  $W_r(\text{Mg I}\lambda 2852)/W_r(\text{Mg II}\lambda 2796)$  vs.  $f_c$ . The filled and open circles are for systems with and without 21-cm absorption respectively.

sible, we have used the VLBA 5 GHz (rather than VCS 2 and 8 GHz) images whenever available. From this table it appears that the detectability of 21-cm does not depend on the covering factor in this sub-sample. We plot in Fig. 10 the ratio  $R_2$  against the measured covering factor  $f_c$  for systems with (filled circles) and without (open circles) 21-cm detection. It is apparent that while the distribution of  $f_c$  is similar between detections and non-detections,  $R_2$  separates the two very nicely.

A covering factor less than 1 increases the  $3\sigma$  optical depth limit by a factor of  $1/f_c$ . In order to quantify the detection rate of 21-cm absorption we give in the last column of Table 5 the integrated optical depth corrected from partial coverage. We come back to this subsample in the next Section while discussing the redshift distribution of 21-cm absorbers.

## 7 REDSHIFT DISTRIBUTION OF 21-CM ABSORBERS

The number density per unit redshift  $n_{21}(\mathcal{T}_0, W_o, z)$ , of 21-cm systems with integrated optical depth  $\mathcal{T}_{21} \geq \mathcal{T}_0$  and Mg II equivalent width  $W_r \geq W_o$  can be obtained from the number density per unit redshift of Mg II absorbers,  $n_{\text{MgII}}(W_o, z)$ , using the equation,

**Table 7.** Redshift distribution of 21-cm absorbers

Sample (1)	$W_o$ (2)	$\mathcal{T}_0$ (3)	N (4)	$N_{21}$ (5)	C (6)	$n_{21}$ (7)
GMRT ( $z_{\text{abs}} = 1.3$ )	1.0	0.10	9	4	$0.44^{+0.35}_{-0.21}$	$0.114^{+0.094}_{-0.057}$
	0.30	26	3	0.12 $^{+0.11}_{-0.06}$	0.030 $^{+0.030}_{-0.017}$	
	0.50	33	4	0.12 $^{+0.10}_{-0.06}$	0.031 $^{+0.026}_{-0.016}$	
	0.50 <sup>a</sup>	12	2	0.17 $^{+0.22}_{-0.11}$	0.044 $^{+0.057}_{-0.028}$	
Low- $z$ ( $z_{\text{abs}} = 0.5$ )	1.8	0.30	14	1	0.07 $^{+0.16}_{-0.06}$	0.006 $^{+0.013}_{-0.005}$
	0.50	20	2	0.10 $^{+0.13}_{-0.07}$	0.008 $^{+0.010}_{-0.006}$	
	1.0	0.30	9	5	0.56 $^{+0.38}_{-0.24}$	0.079 $^{+0.053}_{-0.035}$
	0.50	11	4	0.36 $^{+0.29}_{-0.17}$	0.051 $^{+0.042}_{-0.025}$	
1.8	0.30	6	4	0.67 $^{+0.53}_{-0.32}$	0.023 $^{+0.020}_{-0.012}$	
	0.50	7	4	0.57 $^{+0.45}_{-0.27}$	0.020 $^{+0.017}_{-0.011}$	

Col. 1: Sample name and mean redshift; col. 2: Equivalent width limit; col. 3: Threshold of  $\int \tau \text{dv}$  in  $\text{km s}^{-1}$ ; col. 4: Number of systems in the sample with  $\int \tau_{3\sigma, 10\text{dv}} \leq \mathcal{T}_0$ ; col. 5: Number of 21-cm absorption detections with integration line depth  $\int \tau \text{dv} \geq \mathcal{T}_0$ ; col. 6: Fraction of Mg II systems with detectable 21-cm absorption; col. 7: Number density per unit redshift of 21-cm absorbers with  $\int \tau \text{dv} \geq \mathcal{T}_0$ .

<sup>a</sup> considering only the subsample in Table 5.

$$n_{21}(\mathcal{T}_{21} \geq \mathcal{T}_0, W_r \geq W_o, z) = C \times n_{\text{MgII}}(W_r \geq W_o, z). \quad (3)$$

Where,  $C$  is the fraction of Mg II systems with  $W_r(\text{Mg II} \lambda 2796) \geq W_o$  that show detectable 21-cm absorption.

The redshift incidence of Mg II absorbers can be approximated as,

$$n_{\text{MgII}}(W_o, z) = n_0 \times (1+z)^\gamma \quad (4)$$

with  $n_0 = 0.080^{+0.015}_{-0.005}$  and  $\gamma = 1.40 \pm 0.16$  for  $W_o = 1\text{\AA}$  and  $n_0 = 0.016^{+0.005}_{-0.003}$  and  $\gamma = 1.92 \pm 0.30$  for  $W_r \geq 1.8\text{\AA}$  (Prochter et al. 2006). Therefore at  $\langle z_{\text{abs}} \rangle = 1.3$ , the mean redshift of our sample, we derive,  $n_{\text{MgII}}(W_o = 1\text{\AA}, z = 1.3) = 0.257^{+0.092}_{-0.046}$  and  $n_{\text{MgII}}(W_o = 1.8\text{\AA}, z = 1.3) = 0.079^{+0.054}_{-0.030}$ .

The fraction of Mg II systems that show detectable 21-cm absorption with integrated optical depth,  $\mathcal{T}_{21} \geq \mathcal{T}_0$ , is estimated as follows. First we consider only the systems (say N) with radio spectra sensitive enough so that  $\int \tau_{3\sigma} \text{dv} \leq \mathcal{T}_0$ . Since the typical resolution of the Lane's spectra is  $7-10 \text{ km s}^{-1}$  (see below), we have computed the values of the 21-cm  $3\sigma$ -detection limit for a velocity resolution of  $10 \text{ km s}^{-1}$  (see Table 3). Then the number of these systems with detectable 21-cm absorption (referred to as  $N_{21}$ ) is estimated by considering the detections that have integrated line depth,  $\mathcal{T}_{21} \geq \mathcal{T}_0$ . Then  $C$  is given by  $N_{21}/N$  and the error in  $C$  is computed using small number Poisson statistics (Gehrels, 1986). The value of  $n_{21}$  for various sub-samples defined using  $\mathcal{T}_0$  and  $W_o$  are summarised in Table 7. For  $W_o = 1\text{\AA}$  the sub-sample with  $\mathcal{T}_0 = 0.5$  contains 33 Mg II systems. About 12% of these systems are 21-cm absorbers. If we restrict ourselves to compact QSOs with VLBA measurements, and use  $\mathcal{T}_0$  corrected for partial coverage (see Table. 5), we find that 17% of these systems are 21-cm absorbers. Thus uncertainties due to unknown covering factor should have little effect on our conclusions.

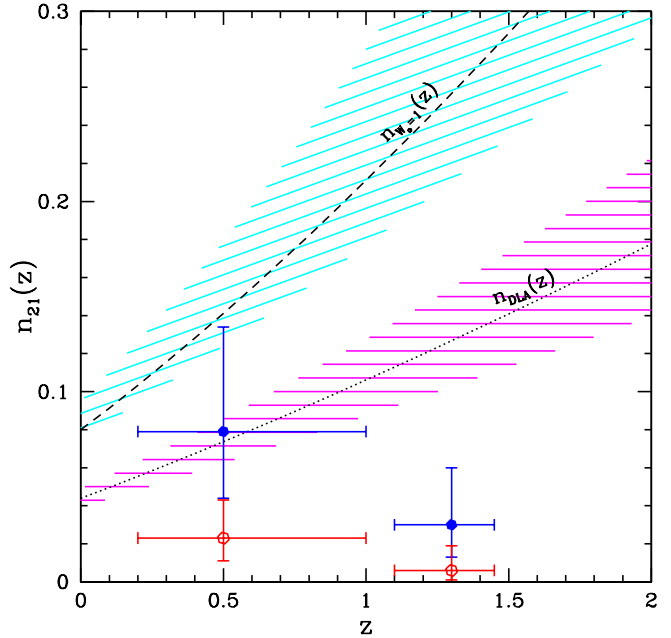


**Figure 11.** Number of 21-cm absorbers per unit redshift,  $n_{21}(z)$ , for integrated 21-cm optical depth,  $\mathcal{T}_0 > 0.3$  and  $W_o(\text{Mg II}) > 1.0\text{\AA}$  (solid symbols) and  $W_o(\text{Mg II}) > 1.8\text{\AA}$  (open symbols). Lines and hashed areas show the number of absorbers per unit redshift for DLAs (RTN06, dotted line) and Mg II absorbers with  $W_o \geq 1\text{\AA}$  (P06, dashed line).

We use the sample of Lane (2000, see Table 6) to study the redshift evolution of  $n_{21}$ . For two of the systems in this sample ( $z_{\text{abs}} = 0.524$  towards 0827+243 and  $z_{\text{abs}} = 0.5313$  towards 1629+120) we use the results of better quality GMRT observations by Kanekar et al. (2003). In the case of the system at  $z_{\text{abs}} = 0.6560$  towards 1622+238, the 21-cm absorber detected by Curran et al. (2007) is most probably located in front of the extended lobes. As we have avoided such systems in our sample, we do not include it in our statistical analysis. The values of  $n_{21}$  for this sub-sample with  $\langle z \rangle \sim 0.5$  are given in Table 7.

From Table 4 of Prochter et al. (2006) we expect the number density of Mg II systems with  $W_o = 1.0$  and  $1.8\text{\AA}$  to increase by a factor of 1.8 and 2.3 respectively between  $z = 0.5$  and  $1.3$ . If physical conditions in Mg II absorbers (like  $N(\text{H I})$  and CNM fraction) do not change with redshift we expect  $C$  to remain constant and therefore  $n_{21}$  to increase with redshift. This is not the case however. It is clear from Table 7 that, for a given value of  $W_o$  and  $\mathcal{T}_0$ ,  $C$  is less at higher  $z$ . This decrease is even more pronounced for higher equivalent width ( $W_r(\text{Mg II} \lambda 2796) \geq 1.8\text{\AA}$ ). As the decrease in  $C$  is stronger than the increase in the number of Mg II systems per unit redshift interval we find  $n_{21}$  decreases with redshift.

Rao, Turnshek & Nestor (2006) give the number of DLAs :  $n_{\text{DLA}}(z = 0.609) = 0.079 \pm 0.019$  and  $n_{\text{DLA}}(z = 1.219) = 0.120 \pm 0.025$  suggesting a factor 1.5 increase in the number per unit redshift of DLAs. The number of 21-cm absorbers with  $W_o > 1\text{\AA}$  and  $\mathcal{T}_0 > 0.3$  matches well the number of DLAs at  $z \sim 0.5$  but it is a factor of 4 smaller at  $z \sim 1.3$  (see Fig. 11).

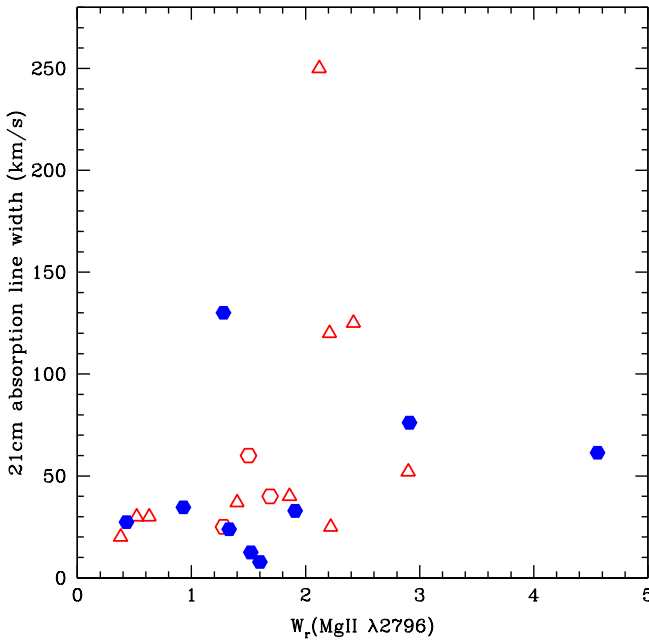


**Figure 12.** Width of the 21-cm absorption as a function of the  $Mg\text{ II}\lambda 2796$  rest equivalent width. Filled hexagons are for our GMRT sample, open triangles for the low- $z$  sample and open hexagons for  $z > 1.8$  DLAs.

The decrease in  $n_{21}$  with redshift can be a consequence of the evolution of H I column density in the Mg II absorbers or lower CNM covering factor at high redshift which may reflect a strong evolution either in the filling factor of the neutral cold gas or the  $f_c$  of the radio sources. From Table 7, it is apparent that the fraction of 21-cm absorbers is not larger for  $W_r(Mg\text{ II}\lambda 2796) \geq 1.8 \text{ \AA}$  compared to  $W_r(Mg\text{ II}\lambda 2796) \geq 1 \text{ \AA}$  at  $z \sim 1.3$ . This is counter-intuitive as RTN06 have found that the fraction of DLAs amongst Mg II systems increases with increasing  $W_r(Mg\text{ II})$  (see their Fig. 6). Now the  $T_o = 0.3$  corresponds to  $\log N(\text{H I}) = 19.74$  for the  $T_s = 100$  K. From the sample of RTN06 we find that the fraction of  $W_r \geq 1 \text{ \AA}$  systems with  $\log N(\text{H I}) \geq 19.74$  for the  $z_{\text{abs}} \leq 1.0$  and  $z_{\text{abs}} > 1.0$  is  $50 \pm 10\%$  and  $75 \pm 15\%$  respectively. Thus the decrease in  $n_{21}$  for  $T_o = 0.3$  is unlikely to be due to the evolution in column density amongst the Mg II absorbers. Further we have shown that the fraction of 21-cm absorbers in our sample does not depend strongly on radio morphology (see Table 7). The available data are therefore consistent with the CNM fraction of neutral H I in Mg II systems being smaller at higher redshifts. This will also be consistent with the results of Ménard et al. (2008) who found the dust content of the strong Mg II absorbers to be increasing with the cosmic time over the redshift range of  $0.4 < z < 2.2$ .

## 8 VELOCITY SPREAD OF 21-CM ABSORPTION

In this Section we investigate any possible correlation between the velocity width of the 21-cm absorption and the  $Mg\text{ II}\lambda 2796$  rest equivalent width. Indeed, Lane (2000) suggested that systems with large metal line equivalent widths

**Table 8.** Results of non-parametric and rank correlation tests.

Sample*	$\rho$	$\tau$	Probability	$\sigma$
(1)	(2)	(3)	$\rho$	$\tau$
GMRT(9)	0.133	0.056	0.732	0.835
GMRT-J0804+3012(8)	0.429	0.214	0.289	0.457
GMRT +high- $z$ (12)	0.165	0.092	0.608	0.676
low- $z$ (10)	0.596	0.494	0.069	0.046
low- $z$ -0809+483	0.678	0.592	0.045	0.026
All(22)	0.482	0.337	0.023	0.028
All-0804-0809(20)	0.573	0.411	0.008	0.011

\*Numbers in brackets correspond to the number of 21-cm absorbers in the subsamples.

could be associated with multi-component 21-cm absorption. In addition, using mostly the sample described in Lane (2000), Curran et al. (2007) have reported a correlation (significant at the  $2.2-2.8\sigma$  level) between the 21-cm line width and the  $Mg\text{ II}\lambda 2796$  equivalent width.

In order to probe the presence of such a correlation in our sample we computed the 21-cm velocity width using the apparent optical depth profile and the method described in Ledoux et al. (2006) for the low ionization metal lines (see Section 5 and Fig. 6). Even though our parent sample of Mg II systems has a wide range in  $W_r(Mg\text{ II}\lambda 2796)$  most of our 21-cm detections correspond to systems with widths of 1-2 Å. However, we find that measured 21-cm absorption velocity width ranges from 7 to 130 km/s (Table 4).

In Fig. 12 we plot the 21-cm line width as a function of  $W_r(Mg\text{ II}\lambda 2796)$ . Filled hexagons are for our GMRT sample, open triangles for the low- $z$  sample and open hexagons for  $z > 1.8$  DLAs. Results of non-parametric and rank correlation tests are summarized in Table 8.  $\rho$  and  $\tau$  are the Spearman and Kendall rank correlation coefficients respectively. The probability for the measured correlation to happen by chance is given in the 4th and 5th columns. The last column gives the significance of the correlation assuming the statistics to be Gaussian for the spearman rank correlation test.

We do not find any significant correlation between  $W_r$  and the 21-cm velocity width in the GMRT sample. The largest 21-cm velocity spread is seen towards J0804+3012. Since the velocity spread could be due to the complex structure of the radio source that is resolved in our GMRT map (see discussions in Section 5) we removed this system from the analysis. The possible correlation is stronger but still not significant ( $\lesssim 1\sigma$  assuming statistics to be Gaussian). Adding 3 high- $z$  21-cm absorbers (open hexagons in Fig. 12) observed at  $1.8 < z < 2.1$  for which Mg II equivalent widths are known does not modify the original conclusion of no correlation ( $\lesssim 1\sigma$ ). These 3 21-cm absorbers are  $z_{\text{abs}} = 2.0394$  towards 0458-020 (Wolfe et al. 1985; Wolfe et al. 1993),  $z_{\text{abs}} = 1.9440$  towards 1157+014 (Wolfe & Davis 1979) and  $z_{\text{abs}} = 1.7763$  towards 1331+170 (Wolfe & Davis 1979; Briggs et al. 1983).

The results for the low- $z$  data are plotted as open triangles. Here, we use the 6 21-cm absorbers from the low- $z$  sample discussed in the previous Section (see Table 6) plus 4 additional 21-cm absorption systems with Mg II equiva-

lent width measurements. These four additional systems are  $z_{\text{abs}}=0.2213$  towards 0738+313 (Lane et al. 1998; Kanekar et al. 2001),  $z_{\text{abs}}=0.4368$  towards 0809+483 (Aldcroft et al. 1994; Briggs et al. 2001),  $z_{\text{abs}}=0.2377$  towards 0952+179 (Lane 2000; Kanekar et al. 2001) and  $z_{\text{abs}}=0.692$  towards 1328+307 (Davis & May 1978; Cohen et al. 1994). The correlation in this low- $z$  sample (with or without 0809+483 which has a 21-cm velocity width of  $150 \text{ km s}^{-1}$ ) is  $\sim 2\sigma$  significant. There is therefore a difference between low and high redshift. The weak correlation ( $2-2.5\sigma$  level for a Gaussian distribution) noted by Curran et al (2007) is present when we consider the full-sample i.e. all the sources at low and high redshift together.

The main differences between low- $z$  and GMRT samples are (i) a paucity of 21-cm absorption systems with  $W_r(\text{Mg II}\lambda 2796) < 1 \text{ \AA}$  and (ii) a lack of 21-cm absorbers among Mg II systems with  $W_r(\text{Mg II}) > 1.8 \text{ \AA}$  in the GMRT sample. While the first difference is probably related to our sample selection the second difference is probably due to a true evolution in the physical state of the Mg II systems with redshift (see discussion in the previous Section). Therefore we think it is not wise to mix the absorbers at low and high redshifts.

The absence of strong correlation between the total Mg II equivalent width and the 21-cm absorption width is consistent with the idea that the Mg II equivalent width is mostly correlated with the overall kinematics of the gas in the absorbing system and not with the column density in the component associated with the cold gas. In the case of J2340-0053 where we have access to high resolution echelle spectra, we find that the 21-cm absorption is not associated with the strongest metal line component (see Fig. 9). In addition as pointed out by Gupta et al. (2007) we usually find that the 21-cm absorption redshift is slightly different (within  $70 \text{ km s}^{-1}$ ) from the mean redshift defined by the metal absorption lines in the SDSS spectrum. This can again be explained if the 21-cm absorption does not originate from the strongest metal line components that define the absorption redshift at low resolution.

## 9 SUMMARY AND DISCUSSION

We have reported the results of a systematic GMRT survey of 21-cm absorption in a representative sample of strong Mg II systems selected from the SDSS spectra in the redshift range  $1.10 \leq z \leq 1.45$ . We have performed GMRT observations of  $\sim 70\%$  (resp. 35%) of our initial sample of Mg II systems detected in DR5 with  $W_r(\text{Mg II}\lambda 2796) \geq 1 \text{ \AA}$  located in front of compact radio sources with flux density  $\geq 100 \text{ mJy}$  (resp. in the range 50-100 mJy). We show that our observed sample is representative of the full parent population.

We report detection of 9 new 21-cm absorption systems out of 35 systems observed in our survey. This is by far the largest number of systems detected in a single systematic survey in a narrow redshift range. Two of these systems also show  $2175 \text{ \AA}$  dust feature at the redshift of the absorbers (Srianand et al. 2008b). We provide spectra of all non-detections with upper limits on the 21-cm optical depth.

We study the dependence of detectability of 21-cm absorption on different properties of the UV absorption lines detected in the SDSS spectra. We find that if absorption

systems are selected with a Mg II doublet ratio,  $\text{DR} < 1.3$ , and a ratio  $W_r(\text{Mg I})/W_r(\text{Mg II}) > 0.3$ , the success rate for 21-cm detection is very high (up to 90%). We notice that the detections found in a low- $z$  sample by Lane (2000) also obey these joint constraints. Low value of DR and high values of  $W_r(\text{Mg I})/W_r(\text{Mg II})$  in a system will mean a high column density of Mg II and high neutral fraction. Thus this selection favors objects with high  $N(\text{H I})$ . In our sample, we find an apparent paucity of 21-cm absorption among systems with  $W_r(\text{Mg II}\lambda 2796) > 1.8 \text{ \AA}$ , the median  $W_r$  of our sample. This is contrary to what has been seen at low- $z$  (Lane 2000). Interestingly most of these high  $W_r$  systems have high DR and low values of  $W_r(\text{Mg I})/W_r(\text{Mg II})$ . This strongly suggests that the equivalent width in these systems is dominated by velocity spread and not by line saturation.

We discuss the number of 21-cm absorption systems per unit redshift interval for a given limiting value of the integrated 21-cm optical depth and  $W_r(\text{Mg II}\lambda 2796)$ . We show that the fraction of Mg II systems with 21-cm absorption and the  $n_{21}$  decrease from  $z \sim 0.5$  to  $z \sim 1.3$ . The decrease is larger when we use higher equivalent width cut-off. Using a sub-sample of compact sources, with high frequency VLBA observations available, we show that this can not be accounted for by simple covering factor effects. As mentioned above and based on the available data, it appears that most likely the main reason behind this cosmological evolution is the decrease of the CNM covering factor (and volume filling factor) in the strong Mg II absorbers. Indeed, it is known that the number of Mg II systems per unit redshift increases with increasing redshift. The evolution is steeper for stronger systems (Steidel & Sargent, 1992 and P06 for recent reference). Using the data of Steidel & Sargent (1992), Srianand (1996) found that the strongest redshift evolution was seen among the Mg II absorbers with  $W_r(\text{Fe II}\lambda 2383)/W_r(\text{Mg II}\lambda 2796) < 0.5$ . This clearly means the physical conditions in strong Mg II absorbers are different at high and low- $z$ .

Previous surveys (listed in Section 2) have hinted the lack of 21-cm absorption systems at high- $z$  ( $z \geq 2$ ) compared to what is seen at low- $z$ ,  $z \leq 0.5$ . The low detection rate of 21-cm absorption in high- $z$  DLAs is attributed to either the gas being warm (high  $T_s$ ) or to low values of the covering factor because of high- $z$  geometric effects (see Kanekar & Chengalur, 2003 and Curran & Webb, 2006, respectively). In two of our systems (at  $z_{\text{abs}}=1.326$  towards J0850+5159 and  $z_{\text{abs}}=1.209$  towards J0852+3435), the presence of a  $2175 \text{ \AA}$  dust feature allows us to derive an estimate of  $N(\text{H I})$  and therefore  $T_s$  (Srianand et al. 2008b). Both systems have high metallicity, large  $N(\text{H I})$  ( $\sim 6 \times 10^{21} \text{ cm}^{-2}$ ) and  $T_s$  consistent with the temperature in cold neutral (CNM) gas. In the case of the system at  $z_{\text{abs}}=1.361$  towards J2340-0053, the 21-cm line width is consistent with the absorbing gas having  $T \leq 200 \text{ K}$ . Therefore, we already have 3 systems in our sample with properties consistent with the conditions expected for CNM gas. Only 1 such system has yet been detected at  $z \geq 2$  (York et al. 2007). Thus our results are consistent with the increase of the CNM covering factor with decreasing redshift. However, to ascertain this result it would be important to derive  $N(\text{H I})$  directly from the Lyman- $\alpha$  absorption. Thus followup HST/COS observations of a UV bright subsample of our sample is very important to study the redshift evolution of  $T_s$ . As pointed out by nu-

merous authors, the physical state of the gas depends on the star formation activity in the vicinity of the absorber. Models of multiphase interstellar medium suggest that the temperature of different phases depends on the background UV radiation field, metallicity, dust content and cosmic ray density and therefore on the local star formation activity. It is possible to conjecture that the evolution of  $n_{21}$  as a function of redshift is probably related to the fact that at  $z \sim 1.3$  the average SFR in a galaxy is larger than that at  $z \sim 0.5$  so that we expect the CNM fraction to increase with decreasing redshift.

We selected systems with  $W_r \geq 1 \text{ \AA}$  but detected by chance a 21-cm absorption in a system with  $W_r = 0.43 \text{ \AA}$  (at  $z_{\text{abs}} = 1.3710$  toward J0108–0037). Efforts are underway at GMRT to extend our survey to weaker ( $W_r \leq 1 \text{ \AA}$ ) Mg II systems. This will be crucial for understanding the physical state of Mg II systems and to determine the detectability of 21-cm absorption versus  $W_r$ . Ideally one would like to estimate the number density of 21-cm absorbers and measure the cosmological evolution without preselection from the UV absorption lines. This can be achieved only by a blind survey of 21-cm absorption in front of radio loud QSOs. It will be possible to embark upon such a survey with the upcoming Square Kilometer Array (SKA) pathfinders. In particular, the Australian Square Kilometer Array Pathfinder (ASKAP) with its instantaneous wide bandwidth of 300 MHz and large field of view (30 degree $^2$ ) is an ideal instrument for this (Johnston et al. 2008). An ASKAP survey with 150 pointings of 16 hrs each (i.e 2400 hrs in total) in the 700–1000 MHz frequency band would yield detection of  $\sim 100$  to 250 intervening 21-cm absorbers in the redshift range  $0.4 \leq z \leq 1$ .

We have estimated the velocity spread of the 21-cm absorptions using the apparent optical depth method (Ledoux et al. 2006). We do not find any statistically significant correlation between  $W_r(\text{Mg II} \lambda 2796)$  and the 21-cm velocity width in our sample. A marginal correlation is found for the low- $z$  sample. The absence of correlation in the high- $z$  sample is related to the lack of 21-cm absorbers among Mg II systems with  $W_r(\text{Mg II}) > 1.8 \text{ \AA}$  in the GMRT sample. This is probably due to a true evolution with redshift of the physical state of the Mg II systems and consistent with the idea that the Mg II equivalent width is mostly correlated with the overall kinematics of the gas in the absorbing system and not with the column density in the component associated with the cold gas. When high spectral resolution data are available, we note that the 21-cm absorption is not always associated with the strongest Mg II component.

As the energy of the 21-cm transition is proportional to  $x = \alpha^2 G_p / \mu$ , high resolution optical and 21-cm spectra can be used together to probe the combined cosmological variation of these constants (Tubbs & Wolfe, 1980). Using this technique on scanned data, Tzanavaris et al. (2005) obtained  $\Delta x/x = (0.63 \pm 0.99) \times 10^{-5}$ . Our GMRT survey provides systems in a narrow redshift range in which this measurement can be done. Thus high resolution optical spectroscopy of the corresponding QSOs are suitable to perform this test at  $z \sim 1.3$ .

## 10 ACKNOWLEDGEMENTS

We thank Rajaram Nityananda for useful discussions and providing Director's discretionary time on several occasions. We thank the GMRT staff for their co-operation during our observations. The GMRT is an international facility run by the National Centre for Radio Astrophysics of the Tata Institute of Fundamental Research. We acknowledge the use of SDSS spectra from the archive (<http://www.sdss.org/>). RS and PPJ gratefully acknowledge support from the Indo-French Centre for the Promotion of Advanced Research.

## REFERENCES

Aldcroft T.L., Bechtold J., Elvis M., 1994, ApJS, 93, 1  
 Beasley A.J., Gordon D., Peck A.B., Petrov L., MacMillan D.S.,  
 Fomalont E.B., Ma C., 2002, ApJS, 141, 13  
 Briggs F.H., Wolfe A.M., 1983, ApJ, 268, 76  
 Briggs F.H., Wolfe A.M., Liszt H.S., Davis M.M., Turner K.L.,  
 1989, ApJ, 341, 650  
 Briggs F.H., de Bruyn A.G., Vermeulen R.C., 2001, A&A, 373,  
 113  
 Brown R.L., Spencer R.E., 1979, ApJ, 230, L1  
 Carilli C.L., Lane W., de Bruyn A.G., Braun R., Miley G.K.,  
 1996, AJ, 111, 1830  
 Carswell R.F., Strittmatter P.A., Williams R.E., Kinman T.D.,  
 Serkowski K., 1974, ApJ, 190, L101  
 Catinella B., Haynes M.P., Giovanelli R., Gardner J.P., Connolly  
 A.J., 2008, ApJ, 685, L13  
 Cohen R.D., Barlow T.A., Beaver E.A., Junkkarinen V.T., Lyons  
 R.W., Smith H.E., 1994, ApJ, 421, 453  
 Condon J.J., Cotton W.D., Greisen E.W., Yin Q.F., Perley R.A.,  
 Taylor G.B., Broderick J.J., 1998, AJ, 115, 1693  
 Cui J., Bechtold J., Ge J., Meyer D.M., 2005, ApJ, 633, 649  
 Curran S.J., Webb J. K., 2006, MNRAS, 371, 356  
 Curran S.J., Tzanavaris P., Murphy M.T., Webb J.K., Pihlstrom  
 Y.M., 2007, MNRAS, 381, L6  
 Davis M.M., May L.S., 1978, ApJ, 219, 1  
 Ellison S.L., Yan L., Hook I.M., Pettini M., Wall J.V., Shaver P.,  
 2001, A&A, 379, 393  
 Ellison S.L., Ibata R., Pettini M., Lewis G.F., Aracil B., Petitjean  
 P., Srianand R., 2004, A&A, 414, 79  
 Ellison S.L., 2006, MNRAS, 368, 335  
 Fey A.L., Charlot P., 2000, ApJS, 128, 17  
 Fomalont E.B., Frey S., Paragi Z., Gurvits L.I., Scott W.K., Tay-  
 lor A.R., Edwards P.G., Hirabayashi H., 2000, ApJS, 131, 95  
 Ge J., Bechtold J., Kulkarni V.P., 2001, ApJ, 547, L1  
 Gehrels N., 1986, ApJ, 303, 336  
 Gupta N., Salter C.J., Saikia D.J., Ghosh T., Jeyakumar S., 2006,  
 MNRAS, 373, 972  
 Gupta N., Srianand R., Petitjean P., Khare P., Saikia D.J., York  
 D.G., 2007, ApJ, 654, L111  
 Heiles C., Troland T.H., 2003, ApJS, 145, 329  
 Helmboldt J.F., Taylor G.B., Tremblay S., Fassnacht C.D.,  
 Walker R.C., Myers S.T., Sjouwerman L.O., Pearson T.J.,  
 Readhead A.C.S., Weintraub L., et al. 2007, ApJ, 658, 203  
 Hirashita H., Ferrara A., 2005, MNRAS, 356, 1529  
 Hopkins A.M., 2004, ApJ, 615, 209  
 Jannuzi B.T., Bahcall J.N., Bergeron J., Boksenberg A., Hartig  
 G.F., Kirhakos S., Sargent W.L.W., Savage B.D. et al., 1998,  
 ApJS, 118, 1  
 Jackson N., Battye R.A., Browne I.W.A., Joshi S., Muxlow  
 T.W.B., Wilkinson P.N., 2007, MNRAS, 376, 371  
 Johnston S., et al., 2008, ExA, 22, 151  
 Kanekar N., Chengalur J.N., 2001, MNRAS, 325, 631

Kanekar N., Chengalur J.N., 2003, *A&A*, 399, 857

Kanekar N., Subrahmanyan R., Ellison S.L., Lane W.M., Chengalur J.N., 2006, *MNRAS*, 370, L46

Kanekar N., Chengalur J.N., Lane W.M., 2007, *MNRAS*, 375, 1528

Khare P., Kulkarni V.P., Lauroesch J.T., York D.G., Crotts A.P.S., Nakamura, O., 2004, *ApJ*, 616, 86

Kovalev Y.Y., Petrov L., Fomalont E.B., Gordon D., 2007, *AJ*, 133, 1236

Kulkarni S.R., Heiles C., 1988, in Verschuur, G., Kellerman, K., eds., *Galactic and Extragalactic Radio Astronomy* (2nd edition), Springer-Verlag, Berlin and New York, p95

Kunert M., Marecki A., Spencer R.E., Kus A.J., Niegzoda J., 2002, *A&A*, 391, 47

Lah P., Chengalur J.N., Briggs F.H., Colless M., de Propis R., Pracy M.B., de Blok W.J.G., Fujita S.S., Ajiki M., Shioya Y., et al., 2007, *MNRAS*, 376, 1357

Lane W., Smette A., Briggs F., Rao S., Turnshek D., Meylan G., 1998, *AJ*, 116, 26

Lane W., 2000, PhD Thesis, University of Groningen

Lanzetta K.M., Wolfe A.M., Turnshek D.A., 1987, *ApJ*, 322, 739

Lanzetta K.M., Wolfe A.M., Turnshek D.A., 1995, *ApJ*, 440, 435

Lanzetta K.M., McMahon R.G., Wolfe A.M., Turnshek D.A., Hazard C., Lu L., 1991, *ApJS*, 77, 1

Ledoux C., Petitjean P., Srianand R., 2003, *MNRAS*, 346, 209

Ledoux C., Petitjean P., Fynbo J.P.U., Moller P., Srianand R., 2006, *A&A*, 457, 71

Madau P., Ferguson H.C., Dickinson M.E., Giavalisco M., Steidel C.C., Fruchter A., 1996, *MNRAS*, 283, 1388

McKee C.F., Ostriker J.P., 1977, *ApJ*, 218, 148

Ménard B., Nestor D., Turnshek D., Quider A., Richards G., Chelouche D., Rao S., 2008, *MNRAS*, 385, 1053

Noterdaeme P., Petitjean P., Srianand R., Ledoux C., Le Petit F., 2007a, *A&A*, 469, 425

Noterdaeme P., Ledoux C., Petitjean P., Le Petit F., Srianand R., Smette A., 2007b, *A&A*, 474, 393

Noterdaeme P., Ledoux C., Petitjean P., Srianand R., 2008a, *A&A*, 481, 327

Noterdaeme P., Petitjean P., Ledoux C., Srianand R., Ivanchik A., 2008b, *A&A*, 491, 397

Noterdaeme P., et al. 2009, in preparation

Peroux C., McMahon R.G., Storrie-Lombardi L.J., Irwin M.J., 2003, *MNRAS*, 346, 1103

Petitjean P., Bergeron J., 1990, *A&A*, 231, 309

Petitjean P., Srianand R., Ledoux, C., 2000, *A&A*, 364, L26

Petitjean P., Aracil B., Srianand R., Ibata R., 2000, *A&A*, 359, 457

Piner B.G., Mahmud M., Fey A.L., Gospodinova K., 2007, *AJ*, 133, 2357

Prochaska J.X., Herbert-Fort S., Wolfe A.M., 2005, *ApJ*, 635, 123

Prochter G.E., Prochaska J.X., Burles S.M., 2006, *ApJ*, 639, 766

Prochaska J.X., Wolfe A.M., Howk J.C., Gawiser E., Burles S.M., Cooke J., 2007, *ApJS*, 171, 29

Prochaska J.X., Wolfe A.M., 2008, [astro-ph/0811.2003](http://arxiv.org/abs/0811.2003)

Rao S.M., Turnshek D.A., Nestor D.B., 2006, *ApJ*, 636, 610

Reimers D., Baade R., Quast R., Levshakov S.A., 2003, *A&A*, 410, 785

Riley J.M., Warner P.J., 1994, *MNRAS*, 269, 166

Roy N., Chengalur J. N., Srianand R. 2006, *MNRAS*, 365, L1

Srianand R., 1996, *ApJ*, 462, 643

Srianand R., Petitjean P., Ledoux C., 2000, *Nature*, 408, 931

Srianand R., Petitjean P., Ledoux C., Ferland, G., Shaw, G., 2005, *MNRAS*, 362, 549

Srianand R., Gupta N., Petitjean P., 2007, *MNRAS*, 375, 584

Srianand R., Noterdaeme P., Ledoux C., Petitjean P., 2008a, *A&A*, 482, L39

Srianand R., Gupta N., Petitjean P., Noterdaeme P., Saikia D.J., 2008b, *MNRAS*, 391, L69

Steidel C.C., Sargent W.L.W., 1992, *ApJS*, 80, 1

Storrie-Lombardi L.J., McMahon R.G., Irwin M.J., 1996, *MNRAS*, 283, L79

Taylor G.B., Fassnacht C.D., Sjouwerman L.O., Myers S.T., Ulvestad J.S., Walker R.C., Fomalont E.B., Pearson T.J., Readhead A.C.S., Gehrels N., Michelson P.F., 2005, *ApJS*, 159, 27

Teräsraanta H., Wieren S., Koivisto P., Saarinen V., Hovatta T., 2005, *A&A*, 440, 409

Tzanavaris P., Webb J.K., Murphy M.T., Flambaum V.V., Curran S.J., 2005, *PhRvL*, 95d, 1301

Tubbs A.D., Wolfe A.M. 1980, *ApJ*, 236, L105

Varshalovich D.A., Ivanchik A.V., Petitjean P., Srianand R., Ledoux C., 2001, *AstL*, 27, 683

Verheijen M., van Gorkom J.H., Szomoru A., Dwarakanath K.S., Poggianti B.M., Schiminovich D., 2007, *ApJ*, 668, L9

White R.L., Becker R.H., Helfand D.J., Gregg M.D., 1997, *ApJ*, 475, 479

Wolfe A.M., Broderick J.J., Johnston K.J., Condon J.J., 1978, *ApJ*, 222, 752

Wolfe A.M., Davis M.M., 1979, *AJ*, 84, 699

Wolfe A.M., Briggs F.H., 1981, *ApJ*, 248, 460

Wolfe A.M., Briggs F.H., Davis M.M., 1982, *ApJ*, 259, 495

Wolfe A.M., Briggs F.H., Turnshek D.A., Davis M.M., Smith H.E., Cohen R.D., 1985, *ApJ*, 294, L67

Wolfe A.M., Turnshek D.A., Lanzetta K.M., Lu L., 1993, *ApJ*, 404, 480

Wolfe A.M., Lanzetta K.M., Foltz C.B., Chaffee F.H., 1995, *ApJ*, 454, 698

Wolfe A.M., Gawiser E., Prochaska J.X., 2003, *ApJ*, 593, 235

Wolfe A.M., Prochaska J.X., Gawiser E., 2003, *ApJ*, 593, 215

Wolfe A.M., Prochaska J.X., Jorgenson R.A., Rafelski M., 2008, *ApJ*, 681, 881

York, D.G., Khare P., Vanden Berk D., Kulkarni V.P., Crotts A.P.S., Lauroesch J.T., Richards G.T., Schneider D.P. et al., 2006, *MNRAS*, 367, 945

York B.A., Kanekar N., Ellison S.L., Pettini M., 2007, *MNRAS*, 382, 53

Zwaan M.A., Meyer M.J., Staveley-Smith L., Webster R.L., 2005, *MNRAS*, 359, L30